Evolution of biogeochemical Properties Inside Poleward Undercurrent Eddies in the Southeast Pacific Ocean

Lenna O. Ortiz-Castillo[1,2,3], Oscar Pizarro[3,4,9], Marcela Cornejo-D'Ottone[5] and Boris Dewitte[6,7,8]

[1]Centro de Investigaciones en Ecosistemas de la Patagonia (CIEP), Coyhaique, Chile,
[2]Programa de Postgrado en Oceanografía, Departamento de Oceanografía, Facultad de Ciencias Naturales y Oceanográficas, Universidad de Concepción, Chile,
[3]Millennium Institute of Oceanography, Universidad de Concepción, Chile
[4]Department of Geophysics, University of Concepcion, Chile,
[5]Escuela de Ciencias del Mar and Núcleo Milenio para el estudio de la Desoxigenación del Océano Pacífico Sur oriental (DEOXS), Pontificia Universidad Católica de Valparaíso, Valparaíso, Chile,
[6]Centro de Estudios Avanzados en Zonas Áridas (CEAZA), Coquimbo, Chile
[7]Departamento de Biología Marina, Facultad de Ciencias del Mar, Universidad Católica del Norte, Coquimbo, Chile,
[8]CECI, Université de Toulouse III, CERFACS/CNRS, Toulouse, France
[9]Centro de Instrumentación Oceanográfica, Universidad de Concepción, Chile

Correspondence to: Lenna O. Ortiz-Castillo (lenna.ortiz@ciep.cl) and Oscar Pizarro (oscar.pizarro@imo-chile.cl)

Abstract. Oceanic eddies are ubiquitous features of the circulation thought to be involved in transporting water mass properties over long distances from their source region. Among these is a particular type with a core within the thermocline with little surface expression. Despite their significance, their role in the ocean circulation remains largely undocumented from observations. This study characterizes the variations in internal biogeochemistry, disparities with external properties, and processes influencing the dissolved oxygen budget of Poleward undercurrent eddies (Puddies) during their transit to oceanic waters. Employing a high-resolution coupled simulation of the Southeast Pacific, we document biogeochemical properties and processes associated with the nitrogen cycle inside Puddies and contrast them with those of the surrounding environment. Our findings reveal that Puddies capture a biogeochemical signal contingent upon their formation location along the coast, particularly associated with the core of the Peru-Chile Undercurrent at the core of the Oxygen Minimum Zone (OMZ). While permeability at the periphery facilitates exchange with external waters, thereby modulating the original properties, the core signal retains negative oxygen (O_2) anomalies and positive anomalies of other biogeochemical tracers. These anomalous conditions result in tracer values exceeding the 90th percentile of their distribution in the open ocean, in contrast to the formation zones, where anomalies only surpass the 50th percentile. This indicates that Puddies may play a role in modulating the average properties of the open ocean. Suboxic ($O_2 < 20\ \mu M$) cores are prevalent near the coast but decrease in abundance with distance from shore, giving way to a predominance of hypoxic ($20\ \mu M < O_2 < 45\ \mu M$) cores (predominating at 60% in the open sea), suggesting core ventilation during transit. The principal mechanism governing O_2 input into, or output from the eddy core entails lateral and vertical advection, with vertical mixing supplying O_2 to a lesser extent. Biological activity consumes O_2 inside Puddies for around 6 to 12 months, especially intensely for the first 100 days, thus facilitating the persistence of low O_2 conditions and extending the lifetime of biogeochemical anomalies within the core (up to 800 km offshore). The ammonium and nitrite deplete earlier

in the eddy core with a decay rate greater than the nitrate and nitrous oxide, while these are accumulating in open sea (up to 16% and 100% higher than mean state, respectively). Our results suggest that southern regions of the southeast Pacific OMZ undergo greater deoxygenation and nutrient enrichment due to Puddies compared to northern regions. However, the combination of various physical conditions can generate zones with more pronounced changes in the nitrite (subsurface water masses due to interactions with the Puddies, such as at 30ºS. The maximum contribution of NO_2^-) takes place in particular along this latitude, with a 460% increase compared to the mean state, near the coastal zone.

In summary, Puddies formed along the Chilean coast capture distinct biogeochemical "signatures" depending on where they form. In the north, minimal ventilation fosters suboxic conditions and denitrification –leading to deficits of nitrate (NO_3^-) and nitrous oxide (N_2O) but high NO_2^- and ammonium (NH_4^+)– whereas central and southern subregions show increased NO_3^- and higher N_2O. Moreover, cross-shore exchange between Equatorial Subsurface Water and Subantarctic Water further amplifies this variability, giving rise to eddies with diverse nutrient and oxygen properties as they move offshore.

1 Introduction

Oxygen plays a fundamental role for life in the ocean, and numerous processes regulate its concentration in the water column. In subsurface waters (100-800 m depth), oxygen concentrations (O_2) decrease significantly due to the decomposition of organic matter and limited ventilation, leading to the formation of oxygen minimum zones (OMZ) in eastern boundary upwelling systems (EBUS; Wyrtki, 1962; Helly & Levin, 2004; Karstensen et al., 2008; Paulmier & Ruiz-Pino, 2009; Stramma et al., 2010). Under these conditions of low oxygen in the subsurface (i.e. dissolved O_2 less than 20 μM), heterotrophic metabolic processes are important, dominated by activity of bacteria and archaea, resulting in significant shifts in biogeochemical cycles (Lam et al., 2009; Paulmier & Ruiz-Pino, 2009; Wright et al., 2012).

The nitrogen cycle in the oceans involves various chemical species with different oxidation states. Outside the OMZ, where conditions are oxygenated, dinitrogen (N_2) is transformed into ammonium (NH_4^+), nitrite (NO_2^-), and nitrate (NO_3^-) through nitrification, with nitrous oxide (N_2O) produced as a byproduct. However, within the OMZ, where O_2 is depleted, nitrate becomes the primary oxidant, triggering denitrification. In this process, nitrate is reduced to gaseous forms (N_2 and N_2O), which can then be released into the atmosphere. This process has implications for primary production, carbon sequestration, and the release of N_2O into the atmosphere, a potent greenhouse gas (Goreau et al., 1980; Mantoura et al., 1993; Sarmiento & Gruber, 2006; Lam et al., 2009; Paulmier & Ruiz-Pino, 2009; Wright et al., 2012).

The southeast Pacific Ocean is the site of one of the most extensive and shallow OMZs (Paulmier & Ruiz-Pino, 2009), where even anoxic conditions can be observed (Ulloa et al., 2012). Several authors have determined the vertical and zonal (offshore) extent of the OMZ, which exhibits significant seasonal variability, modulated both meridionally by subsurface currents towards the pole, and zonally by mesoscale processes (jets, eddies, fronts, filaments, etc.; Bettencourt et al., 2015; Chaigneau et al., 2011; Grados et al., 2016; Hormazabal et al., 2013; Morales et al., 2012; Stramma et al., 2013; Vergara et al., 2016; Pizarro-Koch

79 et al., 2019). These processes result in changes in water mass properties, and together contribute up to a 25%

80 reduction in O_2 volume during spring (Pizarro-Koch et al., 2019).

81 Furthermore, future projections suggest the expansion of these O_2 depleted zones through global warming

82 (Matear & Hirst, 2003; Stramma et al., 2010; Oschlies et al., 2018) although uncertainties remain (Almendra

83 et al., 2024). The increase in sea surface temperature will affect O_2 solubility, and enhanced water column

84 stratification will impact a range of biological processes that influence O_2 concentrations (Couespel et al.,

85 2019; Keeling et al., 2010; Matear & Hirst, 2003; Oschlies et al., 2018; Schmidtko et al., 2017). In addition,

86 various mechanisms can potentially modify ventilation processes, leading to changes in subsurface water

87 properties. While in current generation climate models, the changes in mean circulation either in the tropics

88 or the high-latitudes, mediated by diapycnal mixing, are invoked to explain the ventilation process (Pitcher et

89 al., 2021), regional modeling studies highlight the importance of mesoscale dynamics, such as mesoscale

90 eddies and zonal jets, in expanding and ventilating oceanic zones with oxygen deficits (Bettencourt et al.,

91 2015; Auger et al., 2021; Calil, 2023). The regional models also provide a more realistic representation of the

92 OMZs than the climate models that do not resolve sub to mesoscale dynamics. This is why understanding the

93 role of mesoscale dynamics on the O_2 and carbon cycles in EBUS has been a key focus of research in recent

94 years.

95 '**P**oleward **u**ndercurrent e**ddies**' (Puddies) are types of subsurface or intrathermocline eddies characterized by

96 coherent anticyclonic lenticular shaped vortices with cores located within the pycnocline and relatively

97 homogenous interior waters (Dugan et al., 1982; McWilliams, 1985; Kostianoy and Belkin, 1989). Puddies

98 originate in the EBUS (Frenger et al., 2018) due to the interaction of the poleward-flowing current with the

99 continental slope, generating submesoscale instabilities with anticyclonic vorticity, subsequently forming

100 these characteristic mesoscale structures (Hormazabal et al., 2013; Combes et al., 2015, Molemaker et al.,

101 2015; Thomsen et al., 2016; Contreras et al., 2019). These eddies represent 30-55% of the anticyclone eddies

102 originating in the EBUS (Pegliasco et al., 2015; Combes et al., 2015) with cores that are warmer, saltier, O_2-

103 depleted, and nutrient-enriched relative to surrounding waters (Collins et al., 2013; Hormazabal et al., 2013;

104 Morales et al., 2012; Johnson and McTaggart, 2010). Therefore, Puddies can play a crucial role in

105 transporting these water properties hundreds or thousands of kilometers offshore to subtropical gyres,

106 potentially contributing to the expansion of the OMZ beyond the coastal region (Frenger et al., 2018).

107 Observations of low O_2 events in open ocean regions provide support for this idea (Lukas and Santiago-

108 Mandujano, 2001; Johnson and McTaggart, 2010; Cornejo-D'Ottone, 2016; Schütte et al., 2016b; Stramma et

109 al., 2013, 2014; Karstensen et al., 2015), with further evidence of biogeochemical processes typically

110 observed only in the OMZ, such as N_2O production (Cornejo-D'Otonne et al., 2016; Arévalo-Martínez et al.,

111 2016; Grundle et al., 2017) and nitrogen loss through denitrification (Altabet et al., 2012; Löscher et al.,

112 2015). Additionally, the observed O_2 utilization rates within the eddy cores range from 0.29 to 44 nmol O_2 L^{-1}

113 d^{-1}, which is up to 3 to 5 times higher than in the surrounding waters (Cornejo-D'Ottone et al., 2016;

114 Karstensen et al., 2015). There is evidence of harboring microbial communities and metabolisms associated

115 with low-oxygen environments that persist even when the eddies enter highly oxygenated waters, a

116 phenomenon known as the "stewpot effect" (Löscher et al., 2015; Frenger et al., 2018).

117   The Southeast Pacific (SEP) is characterized by extensive subsurface mesoscale eddy activity with radii

118   ranging from ~25 to ~50 km and cores of ~500 m of vertical extent (Chaigneau et al., 2009; Hormazabal et

119   al., 2013; Combes et al., 2015, Frenger et al., 2018). They transport a total volume of approximately 1 Sv (1

120   Sv = ~1x10^6 m^3 s^{-1}) westward with an average velocity of ~2 km d^{-1} (Hormazabal et al., 2013). The cores of

121   these eddies exhibit homogenous salinity profiles (>34.5) and low O$_2$ concentrations (< 1.0 mL L^{-1}), linking

122   them to Equatorial Subsurface Water (ESSW) transported poleward by the Peru-Chile Undercurrent (PCUC;

123   Hormazabal, 2004; Colas et al., 2012; Hormazabal et al., 2013). Generally, the low values of O$_2$ in

124   subsurface eddies is related to higher concentrations of nitrate, phosphate, and silicate (Czeschel et al., 2015).

125   However, under suboxic conditions (O$_2$ < 20 μM), the prevailing anaerobic metabolism is denitrification,

126   where nitrate is utilized as an electron acceptor, leading to increased production of NO$_2^-$ and N$_2$O (Goreau et

127   al., 1980; Mantoura et al., 1993; Lam et al., 2009; Wright et al., 2012). Within these eddies, various

128   biogeochemical processes coexist that are highly sensitive to O$_2$ variations, while physical processes

129   modulate biogeochemical patterns through vertical and lateral mixing, submesoscale stirring, or mass

130   exchange with water masses from different origins through turbulent advection (José et al., 2017; Kartensen

131   et al., 2017; Loveccio et al., 2022).

132   This complexity of processes involved during the life cycle of a Puddy, along with the lack of continuous in

133   situ measurements, limits our understanding of nutrient recycling throughout their lifetime, and the balance

134   between processes controlling the rate of change of O$_2$ and nutrients. In the present study, we aim to

135   characterize the internal biogeochemistry of eddies formed under various low-oxygen conditions in the SEP.

136   We analyze the physical and biogeochemical factors influencing the variability in the lifespan of elements

137   trapped within the Puddies, with a particular focus on those related to the nitrogen cycle, as they travel across

138   the OMZ towards better-ventilated oceanic waters. Specifically, we document the evolution of water mass

139   properties and processes inside Puddies with contrasting initial O$_2$ concentrations (suboxic versus hypoxic) to

140   evaluate their role in maintaining the OMZ. Additionally, we aim to address knowledge gaps in the

141   biogeochemical dynamics of this type of eddy, stemming from the lack of observational data, particularly in

142   the SEP. To quantify the changes Puddies undergo due to their complex dynamics, we use a regional coupled

143   biogeochemical model simulation.

144   Our approach involves a robust statistical analysis of contrasting water mass properties inside and outside the

145   Puddies. First, we characterize the initial biogeochemical signal from their formation to assess how, and to

146   what extent, the biogeochemical properties of Puddy' cores vary across different regions of the SEP. Second,

147   we quantify how these properties influence the subsurface waters through which Puddies travel, evaluating

148   the balance of processes involved.

149   The structure of this study is as follows: Section 2 details the model and methods used for the identification

150   and characterization of Puddies. Section 3 describes the biogeochemical characterization inside and outside

151   the Puddies, changes in the O$_2$ budget, and variations in biogeochemical properties from the coastal to

152   oceanic zones. Section 4 discusses the results, and Section 5 presents the main conclusions and future

153   projections.

154

2 Methods

2.1 Regional biogeochemical coupled model

We used a high-resolution, coupled physical-biogeochemical model simulation of the SEP that considers the main processes involved in the transformation of the water masses relevant to the OMZ variability and the dynamics of the Peru-Chile Undercurrent (PCUC). This current plays a significant role in generating Puddies and in the southward extension of the OMZ in the Peru-Chile EBUS.

The physical dynamics was simulated using the Regional Ocean Modelling System (ROMS), a regional ocean circulation model that solves the primitive equations with free surface and sigma coordinates (Shchepetkin and McWilliams 2005; 2009). ROMS was coupled with the biogeochemical model BioEBUS, specifically developed for Eastern Boundary Upwelling Systems (EBUS) and based on the nitrogen cycle using $N_2P_2Z_2D_2$ model formulation (Koné et al., 2005; Gutknecht et al., 2013a). We adopted the same configuration as specified in several other studies in the region (Dewitte et al., 2012; Vergara et al., 2016; Pizarro-Koch et al., 2019). The model has a spatial resolution of 1/12°, 37 vertical levels. 3-day mean outputs are used, which is suitable for resolving mesoscale features. The overall domain covers the latitudinal range of 12°N to 40°S from the coast to 95°W, although the present study focuses on latitudes off the coast of Chile between 20°S and 40°S (Figure 1a). The simulated period was from 2000 to 2008.
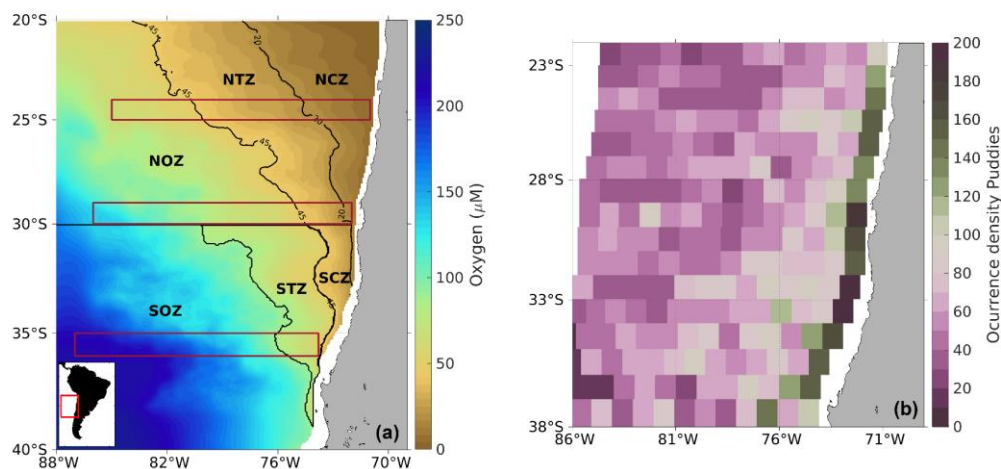

Figure 1. (a) Modeled dissolved O₂ climatology off the Chilean coast, and (b) spatial distribution of the occurrence density of Puddies identified over the nine-year period. Oxygen was considered as being in the isopycnal layer 26.6 kg m⁻³ representative of the OMZ core (defined with S_{core} layer; see Section 2.2). The study area covers 20 - 40ºS and from the coast to 88ºW. The contours used to subdivide regions are based on biogeochemical differences among water masses (see details in Section 2.2). Northern Coastal Zone (NCZ) is delimited by the suboxic zone limit (O₂ = 20 μM); Northern Transition Zone (NTZ) and Southern Coastal Zone (SCZ) separate to 30ºS and the traditional OMZ limit (O₂ = 1mL L⁻¹ or ~ 45 μM), Northern Oceanic Zone (NOZ) with O₂ > 45 μM to northern 30ºS; Southern Transition Zone (STZ) delimited with oxygen contours of 45 μM < O₂ < 90 μM and Southern Oceanic Zone (SOZ) with 90 μM < O₂, both southern 30ºS. Red boxes enclosed the zonal bands taken for made the

181 average compounds by Puddies to 25ºS (from 71ºW to 85ºW), 30ºS (72ºW to 86ºW) and 36ºS (74ºW to 87ºW; see

182 Sections 2.6.2 and 3.4). (Right box) Occurrence density (colormap) is quantified by the total number of Puddies

183 identified in each 1°x1° area for each snapshot (Δt = 3 days), with the possibility that the same eddy may be

184 counted more than once if remaining in the same area. Numbers refer to the total occurrence density by region

185 (see details in Section 2.5).

186

187 The model uses atmospheric momentum forcing data from NCEP-NCAR statistically downscaled based on

188 the QuickSCAT satellite data (see Goubanova et al. (2011) for details). Latent heat flux and other variables –

189 for estimating other air-sea fluxes– such as air temperature and humidity are provided by monthly

190 climatology with a resolution of 1° x 1° from COADS (da Silva et al., 1994). The boundary conditions for

191 temperature, salinity, and horizontal velocity were provided by the SODA 1.4.2 reanalysis (Smith et al.,

192 1992). The BioEBUS model consists of 12 compartments interacting through advection-diffusion equations

193 and source-minus-sink (SMS) processes. The considered components include inorganic dissolved nutrients

194 (NO_3^-, NO_2^-, and NH_4^+), large and small phytoplankton ("small" representing nanophytoplankton; mainly

195 small flagellates between 2 and 20 µm and "large" representing microphytoplankton; mainly diatoms

196 between 20 and 200 µm), large and small zooplankton ("small" representing microzooplankton; mainly

197 heterotrophic ciliates between 20 and 200 µm, and "large" mesozooplankton; mainly copepods between 200

198 µm and 2 mm), and detritus (small and large). Dissolved organic nitrogen (DON) was considered following

199 the formulation of Dadou et al. (2001, 2004) and Huret et al. (2005), O_2 including its ocean-atmosphere

200 interaction according to Peña et al. (2010) and Yakushev et al. (2007), and the production of N_2O using the

201 parameterization of Suntharalingam et al. (2000, 2012). The boundary and initial conditions for the BioEBUS

202 model were obtained from the CARS2006 climatology (CSIRO Atlas of Regional Seas) for O_2 and NO_3^-,

203 with constant vertical profiles adopted for NH_4^+, NO_2^-, and dissolved organic nitrogen (DON) (based on

204 Koné et al. (2005)). The estimated phytoplankton biomass comes from the model. Detailed information on

205 simulation and validation of the physical model (ROMS) is given by Dewitte et al. (2012) and Vergara et al.

206 (2017). The parameter configuration of BioEBUS is the same as that used in Montes et al. (2014).

207 The time rate of change of the concentration of each component is governed by the advection-diffusion

208 equation (see Gutknecht et al., 2013a). For instance, the O_2 balance is given by

209
$$\frac{\partial O_2}{\partial t} = -\nabla \cdot (\vec{u} O_2) + K_H \nabla^2 O_2 + \frac{\partial}{\partial z}\left(K_z \frac{\partial O_2}{\partial z}\right) + SMS(O_2) \qquad (1)$$

210 where $\vec{u} = (u, v, w)$ represents the fluid velocity, with components u for zonal, v for meridional, and w for

211 vertical. The first term on the right-hand side represents the advection (ADV = $-\nabla \cdot (\vec{u} O_2)$), which is a

212 scalar, but can also be decomposed in the sum of zonal (XADV = $-u \frac{\partial O_2}{\partial x}$), meridional (YADV = $-v \frac{\partial O_2}{\partial y}$),

213 and vertical (VADV = $-w \frac{\partial O_2}{\partial z}$) components. The second and third terms correspond to horizontal (HMIX)

214 and vertical (VMIX) diffusion, where K_H is the horizontal eddy diffusion coefficient (set to 100 m^2 s^{-1} in this

215 version of the model), and K_z is the turbulent diffusion coefficient calculated using the K-profile

216 parameterization mixing scheme (Large et al., 1994). The last term $SMS(O_2)$ represents the effect of sources

and sinks associated with biogeochemical processes. For O_2, the source process is primary production, and sink processes include remineralization, nitrification, and zooplankton excretion (Peña et al., 2010).

2.2 Characterization of the study area

The study area extends from 20º to 40ºS and from the Chilean coast to 88ºW. In this region the OMZ core ($O_2 < 45\ \mu M$ or ~ 1 mL/L) is centered at a density surface of $\sigma_\theta = 26.6$ kg m^{-3} (S_{core}) following as reference the core of ESSW near coastal zones, which is similar to Pizarro-Koch et al., (2019; see Section 2.2). S_{core} depth varies, being shallow in the coastal area and deeper in the oceanic region (Table 1). Near the slope, a deepening in S_{core} is observed north of 30°S, where the slope is narrower whereas south of 30°S, it widens.

All variables were interpolated from the original sigma vertical coordinate to depth at 5-meter intervals from 800 m to the surface. In the model, there are 28 vertical levels spanning ~1000 m depth to the surface and 9 vertical levels for depths >1000 m (Figure S1). Regions were selected for averaging tracers and rates, which was based on the characteristic water masses in the region, resulting in domains with irregular shapes (see Figure 1a). The water masses that were considered include primarily the Subantarctic Water (SAAW; also called East-southern Pacific Intermediate Water (ESPIW), characterized here by 11.5°C, 33.8) south of 30°S, where the OMZ is predominantly hypoxic ($O_2 < 45\ \mu M$; as described by Naqvi et al., 2010, and Pizarro-Koch et al., 2019) and significantly narrower. The biogeochemistry of SAAW differs notably from that of Subtropical Water (STW; 20°C, 35.2) north of 30°S, which features a zonally broader OMZ characterized by suboxic conditions ($O_2 < 20\ \mu M$, Figure 2; following Wright et al., 2012), particularly in oxygen, ammonium, and nitrite.

The separation of coastal, transitional, and oceanic zones considered the dominance of Equatorial Subsurface Water (ESSW; 12.5°C, 34.9) in the subsurface waters and its increasing oxygenation farther from the coast (Silva et al., 2009). Given the importance of ESSW in defining the study areas and as the primary water source enclosed in the Puddies, the isopycnal surface associated with the ESSW and OMZ core was used as a reference. Specifically, we focused on the isopycnal with a density of 26.6 kg m^{-3}, corresponding to the reference OMZ core in this model (Pizarro-Koch et al., 2019), which was used in part of our statistical analysis.

We thus came up with 6 subregions: Northern Coastal Zone (NCZ; suboxic conditions); Northern Transition Zone (NTZ; hypoxic conditions); Northern Oceanic Zone (NOZ; with 45 μM < O_2); Southern Oceanic Zone (SOZ; with 90 μM < O_2); Southern Transition Zone (STZ with 45 μM < O_2 < 90 μM) and Southern Coastal Zone (SCZ; hypoxic conditions, Figure 1a).
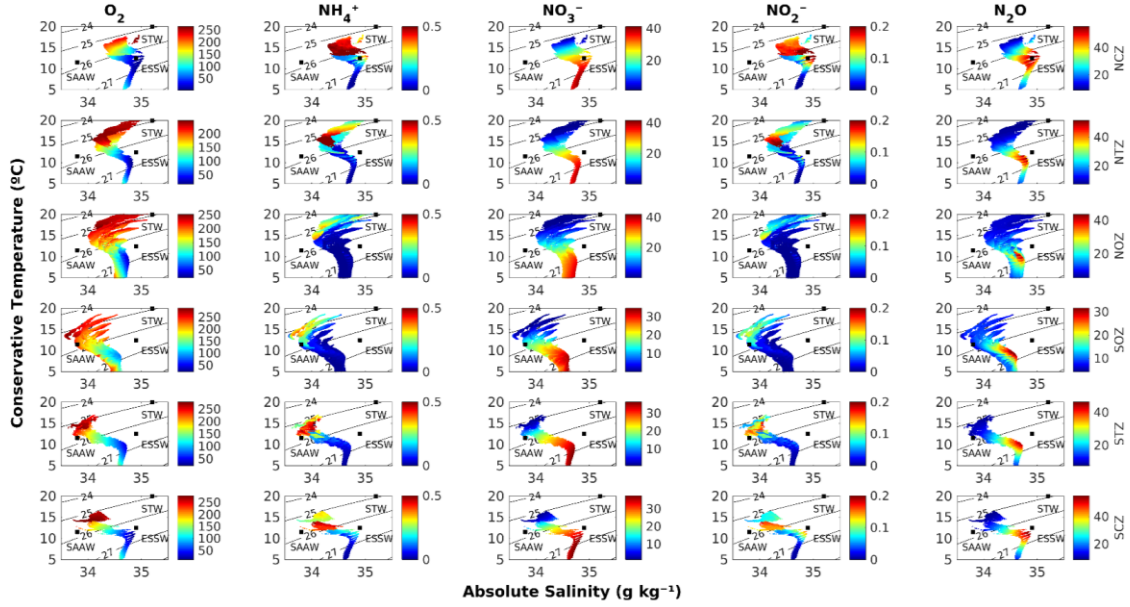
Figure 2. Diagram showing the averages of conservative temperature, absolute salinity, and biogeochemical tracers (in color) for the six study zones (see Figure 1a). The biogeochemical tracers include oxygen (column 1), ammonium (column 2), nitrate (column 3), nitrite (column 4), and nitrous oxide (column 5). From top to bottom the region's names are : Northern Coastal Zone (NCZ); Northern Transition Zone (NTZ); Northern Oceanic Zone (NOZ); Southern Oceanic Zone (SOZ); Southern Transition Zone (STZ) and Southern Coastal Zone (SCZ). The zones' selection is based on the characteristic water masses in the region, primarily the SAAW (Subantarctic Water) south of 30°S, whose biogeochemistry differs significantly from the STW (Subtropical Water) north of 30°S, particularly in oxygen, ammonium, and nitrite. The separation of the coastal, transitional, and oceanic zones considered the dominance of the ESSW in the subsurface waters and its oxygenation away from the coast.

Within the first ~100 km off the coast, the formation zone for Puddies was identified, where a large number of surface and subsurface eddies are typically generated (e.g., Chaigneau et al., 2009) as shown by the occurrence density Puddies (Figure 1b green strip). We considered the total number of Puddies's profiles with a grid box of approximately 1° by 1° in order to characterize the biogeochemical properties of the source water that the Puddies eventually enclose upon formation (see Section 2.6.1).

2.3 Definition of "mean state" and mesoscale contribution

To estimate the physical and biogeochemical perturbations from the mean field associated with the eddies, we use a Reynolds decomposition, which for the field of NO_3^- concentration is written as follows in Eq. (2):

$$NO_3(x,y,z,t) = <NO_3>_{9-year} + NO_3'(x,y,z,t) \tag{2}$$

where $<NO_3>_{9-year}(x,y,z)$ is the "mean state" of NO_3^- calculated as an overall mean across 9 years simulated between the period 2000-2008. Fluctuations of this "mean state" thus consider the large intraseasonal and seasonal variability and are denoted as $NO_3'(x,y,z,t)$. Similarly, for the other variables, $<S>_{9-year}, <NO_2>_{9-year}$, etc., denoted the "mean state", whereas S', NO_2' etc., correspond to anomalies, which includes eddy fluctuations and changes associated with annual and interannual variability. The averages anomalies were denoted as $<S'>, <NO_2'>$, etc., This decomposition method was used for all variables analyzed in each selected subregion (Figure 1a). To evaluate the impacts of the Puddies on the

273 various fields, we used an algorithm to identify subsurface eddies (See details in Section 2.5) and then

274 compared the perturbed fields inside the Puddies with the total field. This latter procedure is further

275 explained in section 2.6.

2.4 Calculation of AOU, ΔNO_3^- and ΔN_2O

277 The apparent oxygen utilization (AOU), NO_3^- production (ΔNO_3^-), and N_2O production (ΔN_2O) provide an

278 estimate of how much has been produced/consumed by biological processes since the water mass was formed

279 in terms of oxygen, nitrate, and nitrous oxide respectively. These estimates are associated with the time the

280 water mass has spent without coming into contact with the ocean surface or being ventilated.

281 The AOU calculation was derived from the García & Gordon (1992) algorithm, based on the O_2 saturation

282 concentration at any temperature and salinity,):

$$AOU = [O_2]_{sat} - [O_2] \tag{3}$$

284 where $[O_2]_{sat}$ is the oxygen saturation and was calculated based on TEOS-10 (using the Gibbs-SeaWater

285 oceanographic toolbox) (https://www.teos-10.org/software.htm), for $[O_2]$ we used the modeled oxygen. The

286 N_2O production (ΔN_2O) was calculated using the Gruber & Sarmiento (2002)'s methodology and the

287 following relationship, Eq. (4):

$$\Delta N_2O = [N_2O] - [N_2O]_{sat} \tag{4}$$

289 where $[N_2O]_{sat}$ is the nitrous oxide saturation calculated from to modeled temperature and salinity, for $[N_2O]$

290 we used the modeled nitrous oxide. NO_3^- production (ΔNO_3^-) is defined as follows,

$$\Delta NO_3^- = [NO_3^-] - [NO_3^-]_{preformed} \tag{5}$$

292 where $[NO_3^-]$ is the modeled nitrate. The value of $[NO_3^-]_{preformed}$ in subsurface waters considered for the

293 above calculation was that of Equatorial Subsurface Water (ESSW), except in SOZ where the value for

294 Antarctic Subsurface Water (SAAW) was taken from Llanillo et al. (2012). The assessment of the modeled

295 O_2, NO_3^- and surface NO_3^- is provided in Appendix.

296

2.5 Puddy Identification

298 For the identification of Puddies, the algorithm proposed by Faghmous et al. (2015) was adapted to deal with

299 subsurface eddies that have a weak dynamical signature at the surface of the ocean. The original algorithm is

300 based on the presence of local extreme values of sea level anomalies (SLA) (minimum in the case of cyclonic

301 eddies and maximum in the case of anticyclonic eddies, considering a neighborhood defined a priori around

302 it). Because the SLA signal from subsurface eddies may be rather weak or absent, the present study used

303 anomalies in the layer thickness (δh) defined as the difference between the depths of the density surfaces

9

304 $S_{upper} = 26.0$ kg m^{-3} and $S_{lower} = 26.9$ kg m^{-3}. Thus, positive anomalies ($\delta h > 0$) indicate the presence of

305 subsurface anticyclonic eddies due to their convex shape (for our case, Puddies). When δh is at its maximum

306 (δh_{max}), the largest closed contour around the geographical location of δh_{max} is considered as the edge of the

307 eddy, as δh_{max} is associated with the center of the eddy and the points contained within the eddy edge are the

308 body of the eddy (Figure S2a; Faghmous et al., 2015). Starting from δh_{max}, a gradual decrease of 0.1 m was

309 used to establish the size and amplitude of the eddy. Only eddies that reached a minimum horizontal area of

310 30 grid points ($A_{min} \sim 1.95 \times 10^9$ m², equivalent to a radius of ~ 25 km) were considered, as eddies below this

311 threshold are not well identified (reducing the total of selected Puddies by 30%). Additionally, only eddies

312 with a radius not exceeding 150 km (~32 pixels in diameter) were included, as larger eddies are also not well

313 detected, with at most three closed-contour structures per snapshot being discarded. This also helps

314 distinguish eddies in coastal regions from other processes, such as coastal trapped waves or upwelling events

315 which occur on larger spatial scales.

316 Eddy identification was performed using 3-day averages across the entire period. Subsequently, all δh_{max}

317 positions were classified by subregion and in 1°x1° cells for their enumeration (Figure 1b) and for

318 characterizing the average properties of these Puddies along the coast (see Section 2.6.1; statistical analyses

319 are shown in section 3).

2.6 Compound Formation

2.6.1 Average Puddies Profiles

322 To understand the typical conditions within Puddies identified in the formation zone and each subregion,

323 average profiles were constructed as follows: i) all eddy centers (i.e., δh_{max} positions) were classified in

324 1°x1° grid cells along the coast and also within the regions defined in Figure 1a, ii) for each eddy center,

325 vertical profiles were extracted between the density surfaces S_{upper} and S_{lower} for all variables, in each

326 corresponding region, iii) then, these profiles were time-averaged to obtain typical profiles for each variable.

327 For the different regions, the values associated with the S_{core} are shown (Section 3.2) to emphasize changes in

328 the ESSW core. The analysis of these results is presented in sections 3.1 and 3.2.

2.6.2 Average zonal compound

330 Based on the identification of eddies over a 9-year period, different latitude bands (25°S, 30°S, and 36°S,

331 Figure 1a) were selected to create a composite constructed from 3D Puddies, considering all the δh_{max} values

332 identified within 1°x1° areas. For these Puddies, we estimated characteristics within the entire eddy volume

333 as follows: i) for each δh_{max} (Puddy center), a mask of the entire volume was created; ii) the area mask was

334 calculated to identify the edge using the Faghmous et al. (2015)'s algorithm, which was found to be most

335 accurate approach (Figure S3; see sensitivity analysis in the Supplementary Material); iii) this mask was

336 applied across all depths (at 5-meter intervals), creating an irregular cylinder between S_{upper} and S_{lower}; iv)

337 from the total volume enclosed by the cylinder, an average vertical profile was obtained at each time step for

338 each variable (see an example of vertical Puddy characterization in Figures S2b-e).

339   A total of 862 Puddies (δh_{max} values) were accounted for in the 25°S zonal band, 810 in the 30°S band, and

340   658 in the 36°S band. Additionally, for each latitude, biogeochemical variables averaged over the 9-year

341   period, representing the mean state (defined in Section 2.3), were used to calculate an average profile

342   associated with a 1°x1° area. Anomalies were then calculated as the difference between these two profiles.

343   The results of this statistical analysis and the subsurface modifications caused by Puddies are presented in

344   Section 3.4.

2.7 Calculation of percentiles

346   To assess the significance of the internal contribution of Puddies relative to the mean state (defined in

347   Section 2.3), we employed a bootstrap method, which involved randomly sampling more than 200 positions

348   in each region and deriving diagnostics. A total of 92 random time steps were selected, and for each time

349   step, 1,000 latitudes and 1,000 longitudes were generated within the domain. These positions were then

350   filtered for each region. The total number of random positions found per region was as follows: 1,246 in

351   NCZ, 1,474 in NTZ, 3,509 in NOZ, 6,808 in SOZ, 521 in STZ, and 235 in SCZ (Table S2).

352   For each obtained position, biogeochemical properties were extracted at the S_{core}. This approach generated an

353   ensemble of values, allowing us to infer the 50th, 75th, and 90th percentiles (P50, P75, P90) used to provide

354   an estimate of significance levels.

3 Results

3.1 Contrasting biogeochemical characteristics inside and outside the Puddies in the formation zone

358   The region within the first ~100 km off the coast was considered a formation zone for Puddies where a large

359   number of surface and subsurface eddies are typically generated (e.g., Chaigneau et al., 2009; Figure 1b,

360   green strip). Approximately 1° of latitude x 1° longitude boxes were selected along the coast to characterize

361   the biogeochemical properties of the source water that the Puddies eventually enclose upon formation (see

362   Section 2.6.1).

363   Over the 9-year study period in the simulated study region (Figure 1a), an average of approximately 14

364   Puddies were observed at each time step, resulting in a total of ~15,340 Puddy profiles (defined as the

365   vertical profile associated with the δh_{max}) identified (see Section 2.5). If the same eddy remained within the

366   same 1°x1° grid area, it was counted multiple times (using a 3-day time step) until the center of the eddy

367   moved to an adjacent 1°x1° grid. The area with the highest density of identified Puddies profiles was

368   concentrated in the coastal region (2,548), within the first ~100 km from shore, with the maximum

369   abundance noted between 29º – 35ºS (Figure 1b). To assess the impact of Puddies along the coastal strip, we

370   evaluated the mean distribution of several variables (salinity, O_2, NO_3^-, NO_2^-, NH_4^+, and N_2O) in areas of

371   approximately 1°x1° along the coast from 20°S to 38°S and between the isopycnal surfaces S_{upper} and S_{lower}

372   that define the OMZ core in the model (see details in Section 2.6.1). Then, we calculated the mean profiles of

373   these variables in the center of the Puddies observed in each discrete coastal area (1°x1°) and estimated

anomalies of the profiles concerning the general mean profile of the corresponding box (Figures 3, see also Figure S4 in the supplementary material).

Meridional changes in water properties along the coastal strip impact the initial properties of the Puddies. In the northern sector (between 20°S and 30°S), the waters are warmer, more saline, and have lower O_2 (Figures 3a, 3d), with higher concentrations of NO_2^- and NH_4^+ (Figures 3j and 3m). In contrast, towards the south (south of 30°S), these characteristics generally show the opposite tendency, consistent with the water properties observed within Puddy cores. However, NO_3^- and N_2O evidence maximum levels in the central region (near 30°S) (Figures 3g and 3p), where eddies with the highest N_2O concentrations are also observed. Oxygen levels were higher at the upper and lower limits of the OMZ (i.e., near $\sigma_\theta = 26.3$ kg m^{-3} and $\sigma_\theta = 26.7$ kg m^{-3}) and remained relatively low in the OMZ core ($\sigma_\theta \sim 26.5$ kg m^{-3}). Both NH_4^+ and NO_2^- anomalies generated by the Puddies showed maximum values in the upper limit of the eddy cores (near $\sigma_\theta = 26.3$ kg m^{-3}; Figures 3k, 3n) and were fairly uniform along the coastal strip, except between 22° - 24°S and the north-central region, which showed slightly higher anomalies (Figures 3k). South of 33°S, in the narrowest part of the OMZ, the largest anomalies in O_2, NO_3^- and N_2O are observed (Figures 3e, 3h, 3q), accompanied by a higher standard deviation (Figures 3f, 3i, 3r).

3.2 Biogeochemical characteristics inside the offshore Puddies

From the total of 15,340 Puddies profiles, statistics over the 6 subregions defined in Section 2.2 (see also Figure 1a) are performed, which is synthesized in Tables 1 to 3. Table 1 provides statistics associated with general characteristics of the subregion, Table 2 presents statistics on ESSW properties, while Table 3 focuses on Puddies' characteristics.

Table 1. General characteristics of the study subregions. The S$_{upper}$ layer refers to $\sigma_\theta = 26.0$ kg m^{-3}, the S$_{core}$ layer refers to $\sigma_\theta = 26.6$ kg m^{-3} and the S$_{lower}$ layer corresponds to $\sigma_\theta = 26.9$ kg m^{-3}. Their average depth was indicated with ($\pm$) representing the errors estimated based on a bootstrap method (see Methods). Mean thickness was defined as the distance between the S$_{upper}$ and S$_{lower}$ isopycnal layers.

Regions	Area (km²)	Depth S$_{upper}$ (m)	Depth S$_{core}$ (m)	Depth S$_{lower}$ (m)	Mean thickness (m)
NCZ	449 550	108±2	267±3	466±4	360
NTZ	655 300	149±3	277±2	449±2	300
NOZ	1 220 800	188±3	305±3	456±3	270
SOZ	1 808 100	176±9	289±10	439±10	260

12

STZ	359 760	151±3	278±3	451±3	300
SCZ	113 600	99±3	256±2	454±4	355

3.2.1 Oxygen and salinity relationship in ESSW

An evaluation of the relationship between average salinity ($< S >_{9-year}$, as a conservative variable) and average oxygen ($< O_2 >_{9-year}$) and average AOU ($< AOU >_{9-year}$) was conducted for each subregion (Table 2). This analysis was performed using the 26.6 kg m^{-3}, where the ESSW core was observed (see Section 2.2).

Each water mass acquires characteristics through physical and biogeochemical processes, producing particular relationships between the physicochemical variables. Low O_2 waters are closely related to relatively salty ESSW waters. In our study region, this water mass is located between two low-salinity and relatively well-ventilated water masses (i.e., SAAW above and AIWW below). Thus, salinity and O_2 show a linear inverse correlation between the upper and lower oxyclines that delimit the OMZ. Nevertheless, the occurrence of biogeochemical processes can disrupt this relationship. Therefore, it is useful to quantify which regions show these nonlinear biogeochemical processes in the context of the hypothesis that a linear relationship between O_2 and salinity corresponds to an aging of the water mass due to lack of ventilation. A nonlinear relationship would imply the presence of other processes, such as denitrification. Linear regression was performed between absolute salinity, O_2, and AOU on the S_{core} surface, where AOU provides a measure of the apparent O_2 consumption since the ESSW formation (Table 2).

Table 2. **Linear regression between average AOU (μM, $< AOU >_{9-year}$) and average salinity (g kg^{-1}, $< S >_{9-year}$), and between average oxygen (μM, $< O_2 >_{9-year}$) and $< S >_{9-year}$ within each subregions in the S_{core} layer (σ_θ = 26.6 kg m^{-3}). Linear correlation coefficient (R^2) provides a measure of how well $< AOU >_{9-year}$ and $< O_2 >_{9-year}$ are accounted for by a linear model where mean absolute salinity is considered a predictor. Error in the parameters' estimate is provided.**

Regions	$< AOU >_{9-year} = a \times < S >_{9-year} + b$			$< O_2 >_{9-year} = a' \times < S >_{9-year} + b'$		
	R^2	a	b	R^2	a'	b'
NCZ	0.88	112.5±0.57	-3664.6±21	0.92	-142±0.6	4963.5±20.1
NTZ	0.85	199.2±1	-6685.2±33.5	0.88	-229±0.9	7998.6±33.4

13

NOZ	0.96	380.3±0.6	-12908±20.3	0.97	-412±0.6	14281±20.4
SOZ	0.75	409.3±1.6	-13893±55.6	0.78	-445.2±1.6	15410±55.6
STZ	0.95	294.5±1	-9989.3±36.2	0.96	-327.1±1	11396±36
SCZ	0.98	200.8±0.7	-6737±25.2	0.99	-232±0.7	8097±25.6

424

425

426
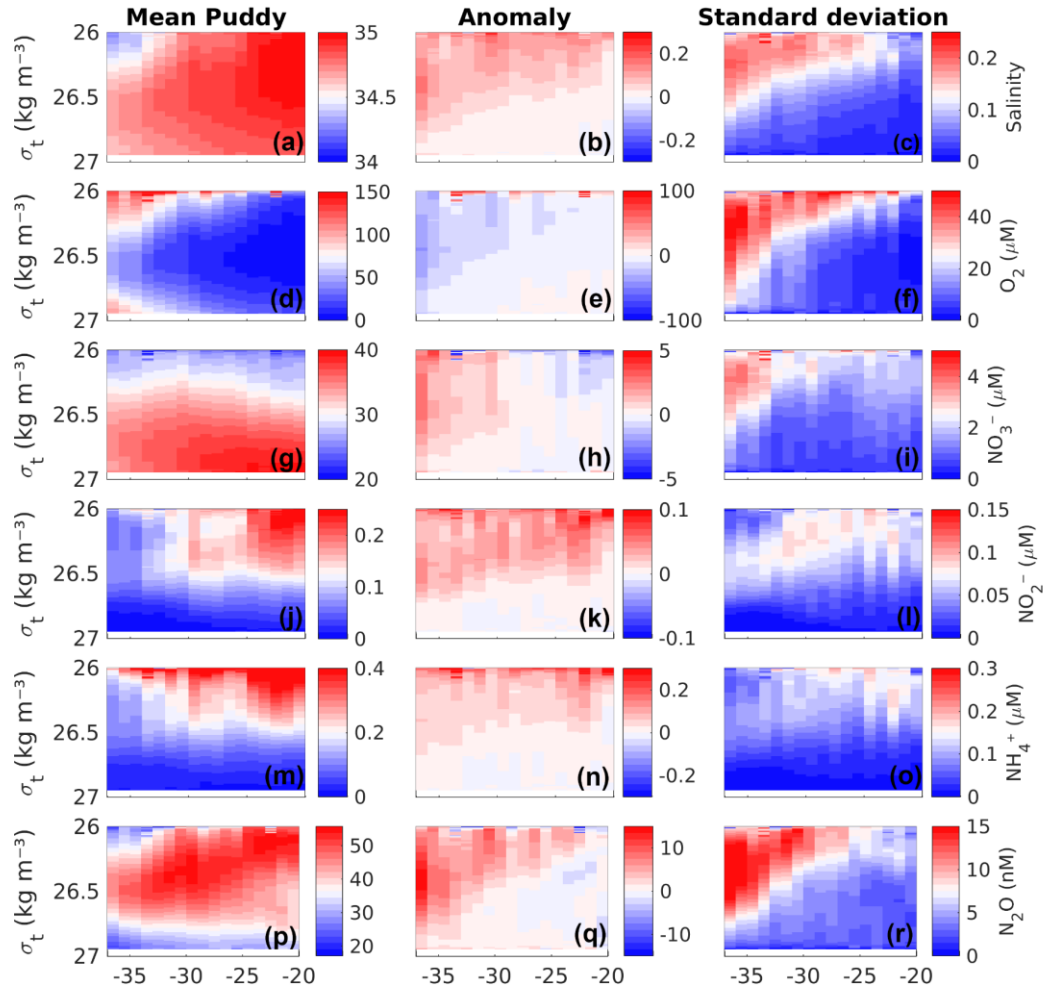
Figure 3. Composite mean vertical profiles (left column), their anomalies relative to the long-term mean (middle column) and the standard deviation of the anomalies (right column) associated with biogeochemical features within the center of the Puddies over the first ~100 km from the slope where there are higher occurrence Puddies (strip in green in Figure 1b). From top to bottom: (a-c) absolute salinity (g kg^{-1}), (d-f) O_2, (g-i) NO_3^-, (j-l) NO_2^-, (m-o) NH_4^+, and (p-r) N_2O. Eddies' mean profiles were obtained by calculating the mean of total profiles identified during nine years in 1°x1° boxes along the coast between the isopycnal layers S_{upper} and S_{lower} (See Methods). The standard deviation is interpreted as the variability of the properties existing at the center. The *x*-axis represents the latitude in degrees, and the *y*-axis shows the potential density anomaly.

435   Oxygen and AOU exhibited a strong linear relationship with absolute salinity ($R^2 > 0.85$) in regions where

436   there is a greater contribution from ESSW (NCZ, NTZ, NOZ, STZ, and SCZ). The slope values ranged from

437   112.5 to 380 for AOU and 142 to 412 for O_2 fit. In contrast, the SOZ exhibited a weaker linear relationship

438   ($R^2 < 0.80$), likely due to the mixing properties of SAAW and AAIW with ESSW (Figure 2, Table S1). SCZ

439   ($R^2 > 0.98$) showed the strongest relationship in the coastal zone, which decreased in NCZ ($R^2 < 0.96$) where

440   denitrification processes have been recorded and there is an evident high value of AOU and a nitrate

441   deficiency (Figures 4a, 4b; Tables 2 and S1). In the northern region, the linear fit improves as it approaches

442   the oceanic zone (NOZ) ($R^2 > 0.96$), indicating a strong presence of the ESSW and a reduced influence from

443   either this biological process or mixing with another water mass.

444

445   **3.2.2 Conditions of Suboxia and Hypoxia in the Oceanic Puddies**

446   We assessed the number of Puddies exhibiting suboxia and hypoxia in each region by identifying the

447   predominant type of low-oxygen cores in coastal, transition, and oceanic zones. The main results are

448   presented in Table 3. The percentage of Puddies exhibiting hypoxia ($O_2 < 45\ \mu M$) and suboxia ($O_2 < 20\ \mu M$)

449   was determined by classifying the range of O_2 concentrations observed in the center of the eddies. The

450   presence of Puddies with these characteristics in the more remote regions was quantified (referred to as NOZ

451   and SOZ in Table 3).

452

453   **Table 3. Percentage of total identified Puddies showing suboxic ($O_2 < 20\ \mu M$) and hypoxic ($20\ \mu M < O_2$**

454   **$< 45\ \mu M$) cores within each region. Total profiles indicated the Puddy profiles identified over the entire**

455   **study period. Mean thickness shown the distance between S_{upper} ($\sigma_\theta = 26.0$ kg m^{-3}) and S_{lower} ($\sigma_\theta = 26.9$**

456   **kg m^{-3}) and δh is the average anomaly thickness generated due to the passage of Puddies in that region**

457   **(i.e. composite δh anomaly).**

458

Regions	Total profiles	Mean thickness (m)	δh (m)	Suboxic cores (%)	Hypoxic cores (%)
NCZ	2,295	475	115	100	0
NTZ	2,114	320	20	70	30
NOZ	3223	325	55	15	66

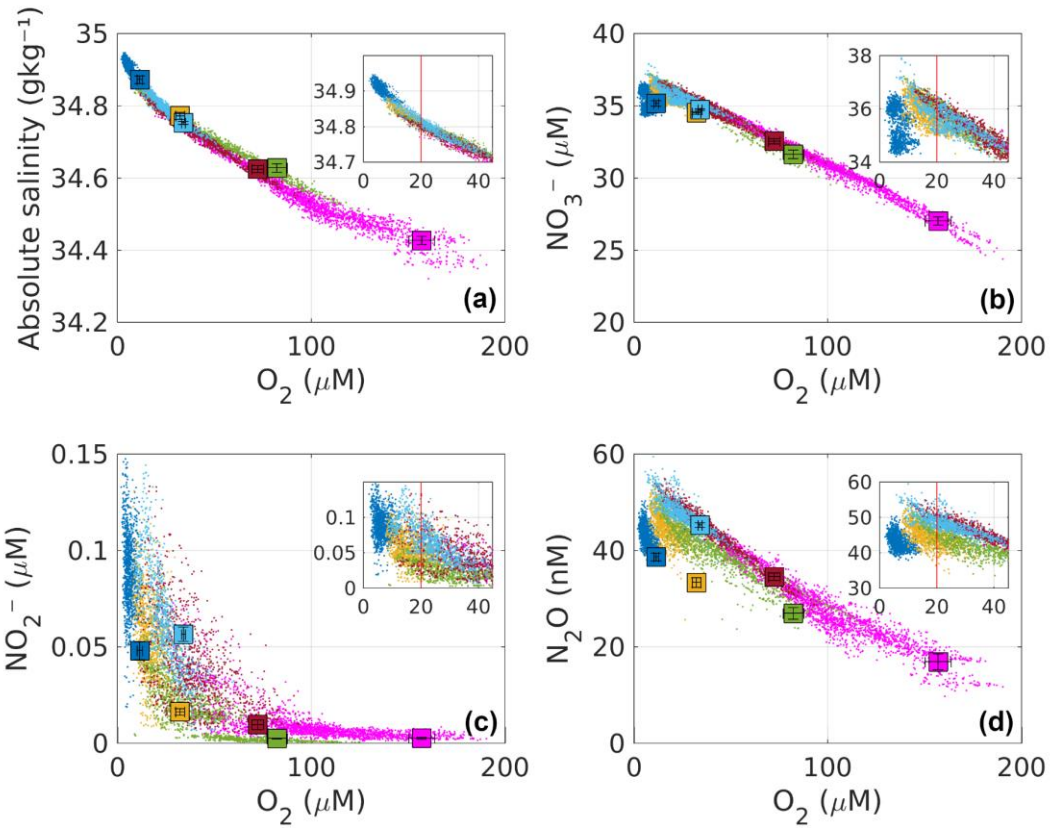|					
SOZ	4781	475	215	<1	9
STZ	1,941	540	240	9	60
SCZ	986	550	195	30	70

459

460
461

462

Figure 4. Relationship between mean O_2 concentration and (a) absolute salinity, (b) NO_3^-, (c) NO_2^-, and (d) N_2O at the S_{core} layer for all identified Puddies. The dots represent the core properties of Puddies (in the S_{core}) of all Puddies identified over a 9-years period, at each timestep. The color indicates the subregion (see Section 2.6.1), which was compared to the mean state value (colored squares, Section 2.3). A positive oxygen gradient is observed from coastal regions (NCZ - dark blue; SCZ - light blue), followed by transition zones (NTZ - yellow; STZ - brown) to the oceanic regions (NOZ - green; SOZ - magenta). Error bars inside the squares correspond to the standard deviation of biogeochemical values within S_{core} for each subregion. The smaller box shows a magnified view of the larger box for hypoxic (20 μM < O_2 < 45 μM) and suboxic (1 μM < O_2 < 20 μM) conditions to highlight . The red line indicates the threshold of O_2 = 20 μM.

472

3.2.3 Differences between biogeochemical properties inside and outside Puddies

To understand the biogeochemical impacts of eddies in oceanic waters, the tracers' values found in the core of the Puddies were compared with the "mean conditions" (Figure S5) of each region in S_{core}. The presence of Puddies manifests a physical change in the mean thickness by the isopycnal layers perturbation during the passage of Puddies, which manifests itself with the average anomaly thickness (δh), different in each subregion (Table 3) and biogeochemical changes with greater contrast observed away from the coast in the south (Figure 4). Values of $< AOU' >, < \Delta NO_3' >$ and $< \Delta N_2O' >$ observed inside the Puddies were higher than $< AOU >_{9-year}, < \Delta NO_3 >_{9-year}$ and $< \Delta N_2O >_{9-year}$ observed outside (Figure 4, 5, 6; Table S1, S2) confirming that eddies maintain hypoxic or suboxic cores that impact regions farther offshore, as shown in the Section 3.2.2 (Table 3).
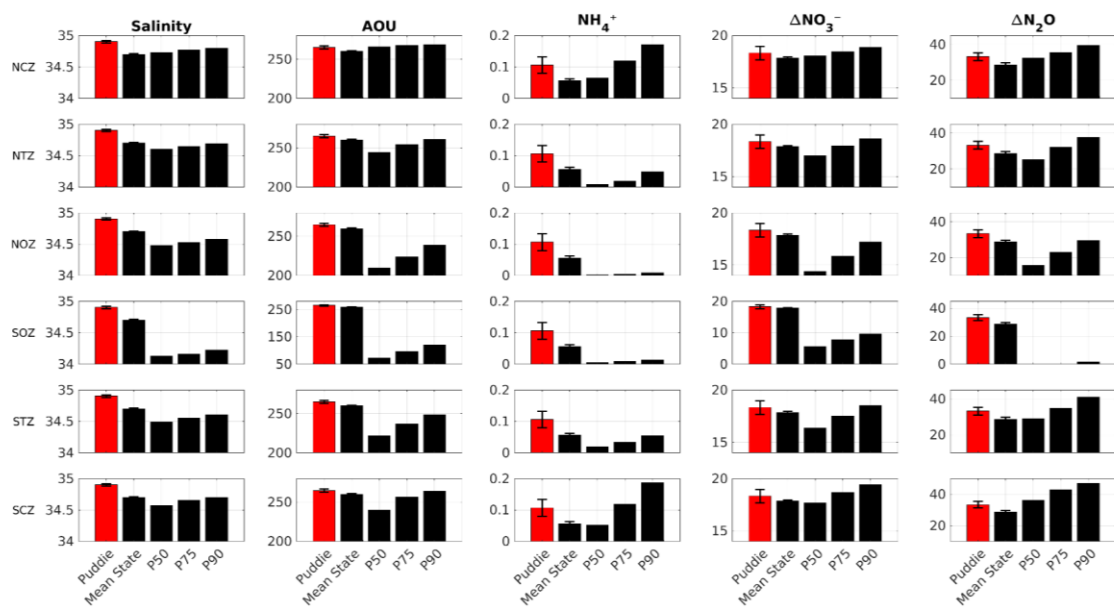
Figure 5. Comparison between the average value associated with all Puddies (red color), the mean state, and the 50th, 75th, and 90th percentiles (black color, P50, P75, P90 respectively) for absolute salinity (g kg⁻¹), AOU, NH₄⁺, ΔNO₃⁻ (µM), and ΔN₂O (nM) in each region (see Section 2.4). The profiles for calculating the percentiles are based on a distribution between 235 to 6800 values - according to the size of the region - obtained from random resampling using Monte Carlo's method (see Section 2.7). The averages were calculated for the S_{core} layer (see Methods) . The errorbar indicates the standard deviation for Puddies and for the mean state (see also Tables S1 and S2 for complementary information).

On the other hand, the asymptotic behavior of NO_2^- was similar to that of NH_4^+ (not show), occurring when $O_2 < 45$ µM (NCZ, NTZ, and SCZ) and tending towards undetectable in regions where $O_2 > 45$ µM (Figure 4c). In SCZ, Puddies with higher concentrations of N_2O than in NCZ (which has suboxic conditions) and NTZ (with hypoxic conditions) can be observed (Figure 4d, Table S1).

In general in the NCZ and SCZ, Puddies maintain the same average salinity, exhibited an increment of 0.5 - 0.7 µM ΔNO_3^- (+2.5 – 4 %), 0.01 up to 0.05 µM NH_4^+ similar to NO_2^- (+12.5 – 83 %), and 3 – 4.5 nM ΔN_2O (+9 – 16 %) associated with an increase of 5 – 9 µM AOU (+2 – 4 %) higher than the mean state (Figures 4

498   and 5; more details, see Table S1). These anomalies were greater than the 50th percentile (P50) for ΔNO_3^-

499   and ΔN_2O and close to the 75th percentile (P75) for AOU and NH_4^+ with salinity exceeding P90 (Figure 5),

500   indicating a significant elevation of biogeochemical elements in the coastal zones due to Puddies compared

501   to the mean state. Offshore, the contrast with the mean state was greater, particularly in the SOZ, reaching

502   100% for NH_4^+, 43% for ΔNO_3^-, 215% for ΔN_2O, 45% for AOU, and 0.3 g kg^{-1} for salinity. These values

503   exceed the P90 (Table S2). Similarly, in the NOZ and STZ, only NH_4^+ exceeded P90, while the rest remained

504   at P75. In NTZ, the AOU and ΔN_2O had values close to or greater than P75, while NH_4^+ and ΔNO_3^- exceeded

505   P90 (Figure 5). The perturbations to the mean state contributed by Puddies in the open sea are more

506   significant than near the coast, although salinity and biogeochemical tracers decrease as the core becomes

507   more oxygenated offshore.

508   The AOU/ΔNO_3^- ratio allows us to quantify the remineralization of organic matter through aerobic processes,

509   which is determined by the Redfield ratio ($R_{N/O}$; 16/138 = 0.11; Redfield et al., 1963). Changes in this

510   relationship indicate the presence of other biological processes that contribute/consume nitrogen in a system,

511   such as nitrogen fixation (ΔNO_3^-/AOU > $R_{N/O}$) and denitrification (ΔNO_3^-/AOU < $R_{N/O}$). On the other hand,

512   the ΔN_2O/AOU ratio provides a measure of N_2O accumulation, so that a high ΔN_2O/AOU is associated with

513   the denitrification process (Sarmiento & Gruber, 2006).

514
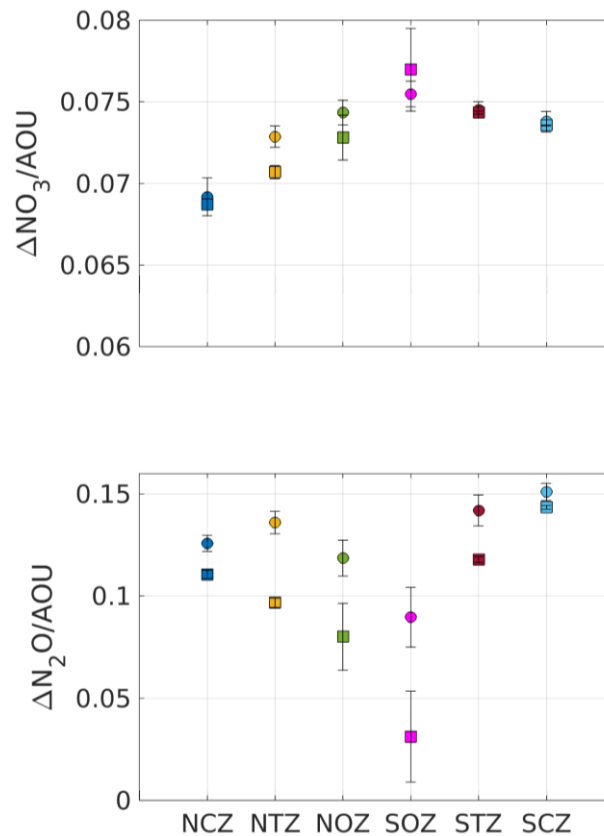
515   **Figure 6. Mean ratios for composite Puddies and mean conditions within each region. (Upper panel) Ratios of**

516   **ΔNO_3^-/AOU. Note that values are smaller than the Redfield ratio ($R_{N/O}$ = 0.11). (Lower panel) Ratios of**

517   **ΔN_2O/AOU. Values of composite Puddies are indicated with a circle while values of the mean state conditions are**

521   We observed a ΔNO$_3^-$/AOU ratio lower than R$_{N/O}$, inside and outside the Puddies (Figure 6, upper box),

522   indicating a deficit of NO$_3^-$ and high O$_2$ consumption due to the elevated remineralization in subsurface

523   waters. The ratio is higher in the suboxic region (NCZ) with an AOU:ΔNO$_3^-$ = 15:1, while in the other

524   regions this signal of old and poorly ventilated waters also extends, albeit in different proportions (Table S1).

525   When $\frac{<\Delta NO_3'>}{<AOU'>} < \frac{<\Delta NO_3>_{9-year}}{<AOU>_{9-year}}$, it must be the case that $< AOU' >$ greater than $< AOU >_{9-year}$ or $<$

526   $\Delta NO_3' >$ is less than $< \Delta NO_3 >_{9-year}$. Since the second assumption is not met, it is true that $< AOU' >$ is

527   greater than $< AOU >_{9-year}$ (Table S1). However, in regions NTZ and NOZ, $\frac{<\Delta NO_3'>}{<AOU'>} > \frac{<\Delta NO_3>_{9-year}}{<AOU>_{9-year}}$,

528   indicating that $< \Delta NO_3' >$ greater than $< \Delta NO_3 >_{9-year}$ or $< AOU' >$ less than $< AOU >_{9-year}$. Given

529   that $< AOU' >$ greater than $< AOU >_{9-year}$, it must have occurred that $< \Delta NO_3' >$ is greater than $<$

530   $\Delta NO_3 >_{9-year}$, so the production of NO$_3^-$ was greater in the Puddies found in these regions compared to

531   others (Table S1). On the other hand, it holds that $\frac{<\Delta N_2O'>}{<AOU'>} > \frac{<\Delta N_2O>_{9-year}}{<AOU>_{9-year}}$. Since $< AOU' >$ greater than $<$

532   $AOU >_{9-year}$, it also follows that $< \Delta N_2O' >$ greater than $< \Delta N_2O >_{9-year}$, therefore the production of

533   N$_2$O was proportionally larger than O$_2$ consumption in the Puddies (Figure 6, lower box; Table S1). Note that

534   although in SCZ and STZ the eddies exhibited the highest values of $\frac{<\Delta N_2O'>}{<AOU'>}$, $\frac{<\Delta N_2O>_{9-year}}{<AOU>_{9-year}}$ was also high

535   (Figure 6). Additionally, the variability of physicochemical conditions in the core increased with distance

536   from the coast and oxygenation.

537   To sum up, according to our model results, Puddies generate significant changes for the mean conditions

538   observed in all regions; particularly large differences were found in AOU and ΔN$_2$O in SOZ. In contrast, the

539   differences in ΔNO$_3^-$ and AOU were not significant in the coastal regions (NCZ and SCZ).

540   **3.3 Oxygen Budget in the Puddies**

541   The processes that contribute to the modulation of the total O$_2$ content are represented in the advection-

542   diffusion equation (Eq. 1, Section 2.1). One part of the equation is associated with O$_2$ changes due to

543   physical processes (referred to as *PHYS*), and another part is related to the production/consumption of O$_2$

544   through biogeochemical processes (*SMS*), so we can write $\frac{\partial O_2}{\partial t} = PHYS + SMS$. PHYS comprises horizontal

545   advective processes (HADV = XADV + YADV), horizontal mixing (HMIX) in the *x-y* plane, vertical

546   advection (VADV), and vertical mixing (VMIX) in the *z*-direction so that PHYS = HADV + VADV + HMIX

547   + VMIX. Note that HMIX and VMIX are mainly related to small-scale (subgrid-scale processes) mixing

548   (e.g., Pizarro-Koch et al., 2019). On the other hand, the SMS (source minus sink processes of O$_2$) includes

549   primary production, remineralization, nitrification, and zooplankton excretion (SMS = PP + Rem + Nitrif +

550   Exc).

551   We analyzed the contribution of each component of the equation to the O_2 balance in the center of the

552   Puddies, dividing the contributions above and below the S_{core} (Figure 7). This was motivated by the fact that

553   there is a significant variance in the upper part of the eddy cores, which is also associated with a large

554   skewness (Figure S6). This indicates a marked vertical variability in the probability density function of the

555   different terms involved in the O_2 balance in the upper part of the eddy cores, probably induced by vertical

556   mixing. Positive (negative) values indicate O_2 increasing/production (decreasing/consumption). In general,

557   we observed that the contribution of PHYS was negative, mainly in the lower part of the eddy, while only

558   NCZ and SCZ positive values dominated at the top, although they were weak, indicating O_2 increasing

559   within the core (Figure 7c). On the other hand, O_2 consumption through SMS (maximum in the transition

560   zones NTZ and STZ) occurred in the upper part of the Puddies (Figure 7f). This proves that elevated

561   biological activity is maintained in the eddies far from shore, with higher intensity in younger eddies but

562   weakening in eddies that reach regions very distant from the coast (NOZ and SOZ). Although the SMS

563   fluxes are of the order $O(10^{-6})$, one order of magnitude lower than the PHYS, small changes in O_2 due to

564   SMS can also result in a sharp local spatial gradient in O_2 that induces strong changes in the advection of O_2.

565   This could significantly impact on the behavior of biogeochemical components that are highly sensitive to

566   minimal changes in O_2 concentration, especially under hypoxic or suboxic conditions.
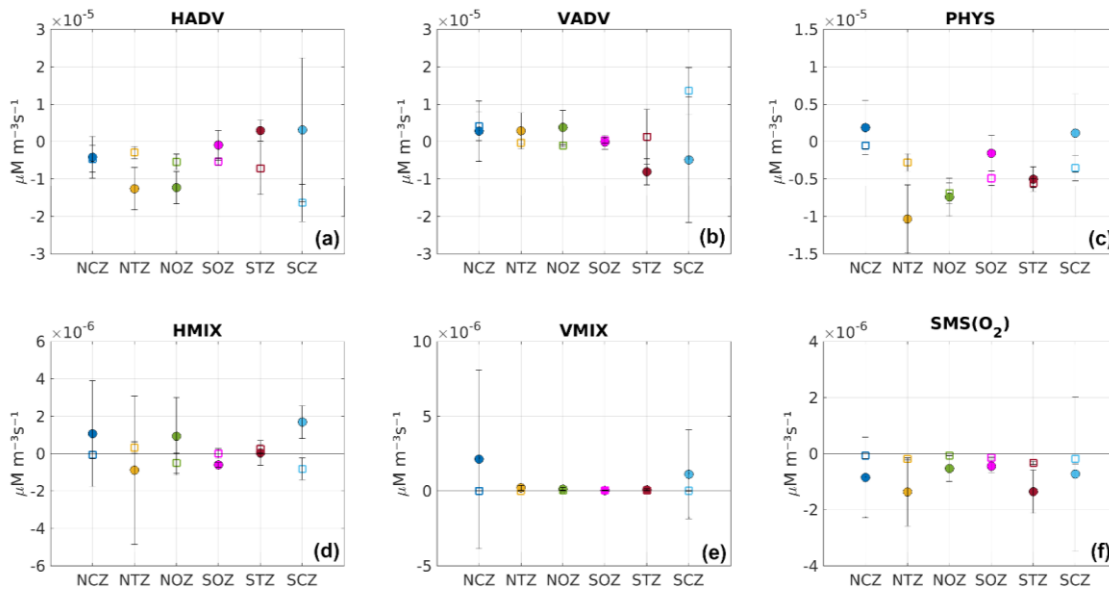

567

568   **Figure 7. Mean terms involved in the O_2 budget (see equation 1). The different terms were temporally averaged**

569   **inside the eddies in each subregion. PHYS is the sum of physical processes, which encompasses horizontal**

570   **advection (HADV = XADV + YADV), vertical advection (VADV), horizontal mixing (HMIX), and vertical mixing**

571   **(VMIX). The biogeochemical processes are included as sources minus sinks (SMS) processes impacting O_2. In**

572   **particular, SMS includes the O_2 fluxes by primary production, nitrification, remineralization, and excretion of the**

573   **zooplankton. Positive (negative) values indicate processes contributing to increasing (depleting) O_2 inside the**

574   **eddy. (a) HADV (b) VADV, (c) PHYS, (d) HMIX, (e) VMIX, and (f) SMS. The averaging was carried out by**

575   **dividing the composite Puddy profile (see Section 2.6.1) into two parts: above (fill circles) and below (squares) the**

576   **26.5 kg/m³ isopycnal surface. This division was based on the marked vertical variability observed in the**

577 **probability density function, as indicated by the variance and skewness (Figure S6). The vertical bars represent**

578 **standard deviations of the O_2 budget terms within S_{core} for each subregion.**

579 The advection components ($O(10^{-5})$) can be interpreted as the ability to maintain O_2 at the center of the eddy

580 during the eddy's displacement. They dominate the O_2 budget compared to mixing processes ($O(10^{-6})$)

581 involving diffusion of O_2 (Figures 7a, 7b). The lateral fluxes (HADV) showed O_2 leakage (HADV < 0) from

582 the core mainly in the northern eddies but not in the southern eddies (HADV > 0), where O_2 influx to the

583 core was evident (Figure 7a). Assuming vertical oxygen advection dominates over shear-induced oxygen

584 transport, in the northern regions, VADV > 0 dominates in the upper part of the Puddies, indicating O_2 input.

585 In contrast, in the southern regions, this pattern is reversed. In coastal zones, vertical advective processes

586 become significant, with VADV > 0, highlighting the greater O_2 input in SCZ (Figure 7b).

587
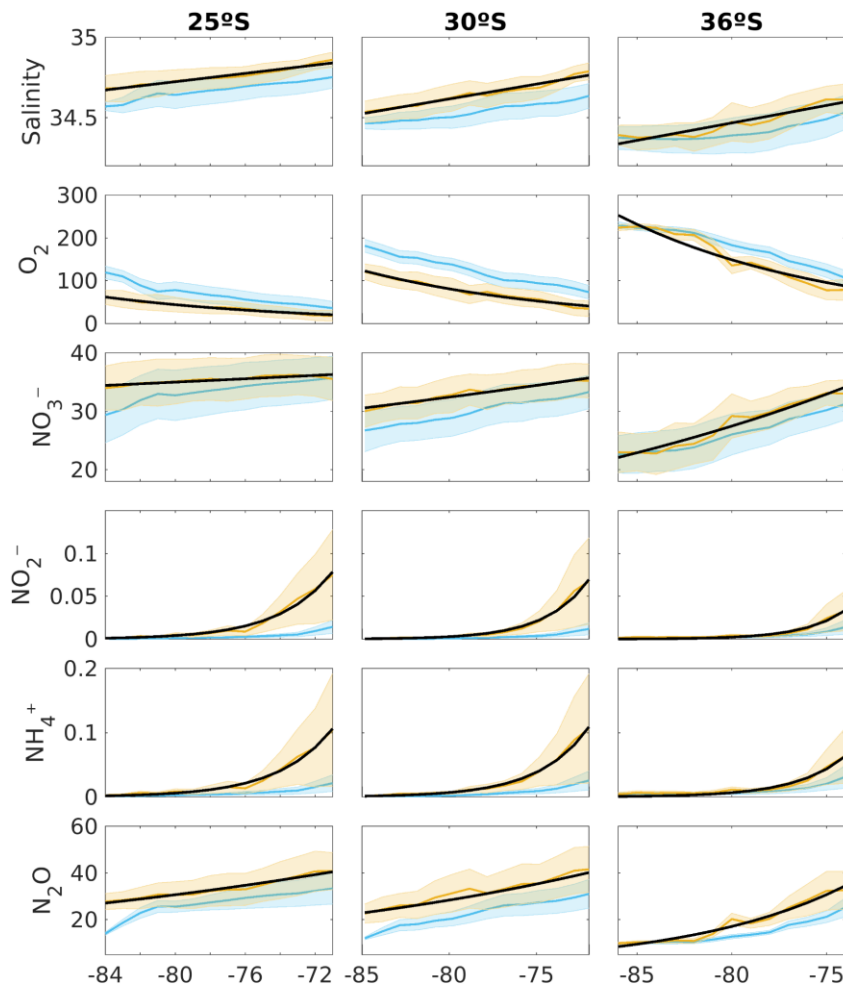
Figure 8. (orange line) Average biogeochemical properties of the total volume of Puddies identified in the zonal bands corresponding to the latitudes of 25°S (left), 30°S (middle), and 36°S (right), and (blue line) the mean state associated with that volume . In order from top to bottom: absolute salinity (g kg^{-1}), oxygen, nitrate, nitrite, ammonium (μM) and nitrous oxide (nM). The *x*-axis shows the longitude in degrees west. At 25°S, 30°S and 36°S 862, 810 and 658 Puddies profiles were considered, respectively. The shading indicates the standard deviation amongst the Puddies. The black line stands for the result of an exponential model of the form $y = Ae^{-kx}$ that provides the decay rate of mean biogeochemical properties as the distance from the coastal zone (see Table 4 for values of *k* for both mean state and Puddies).
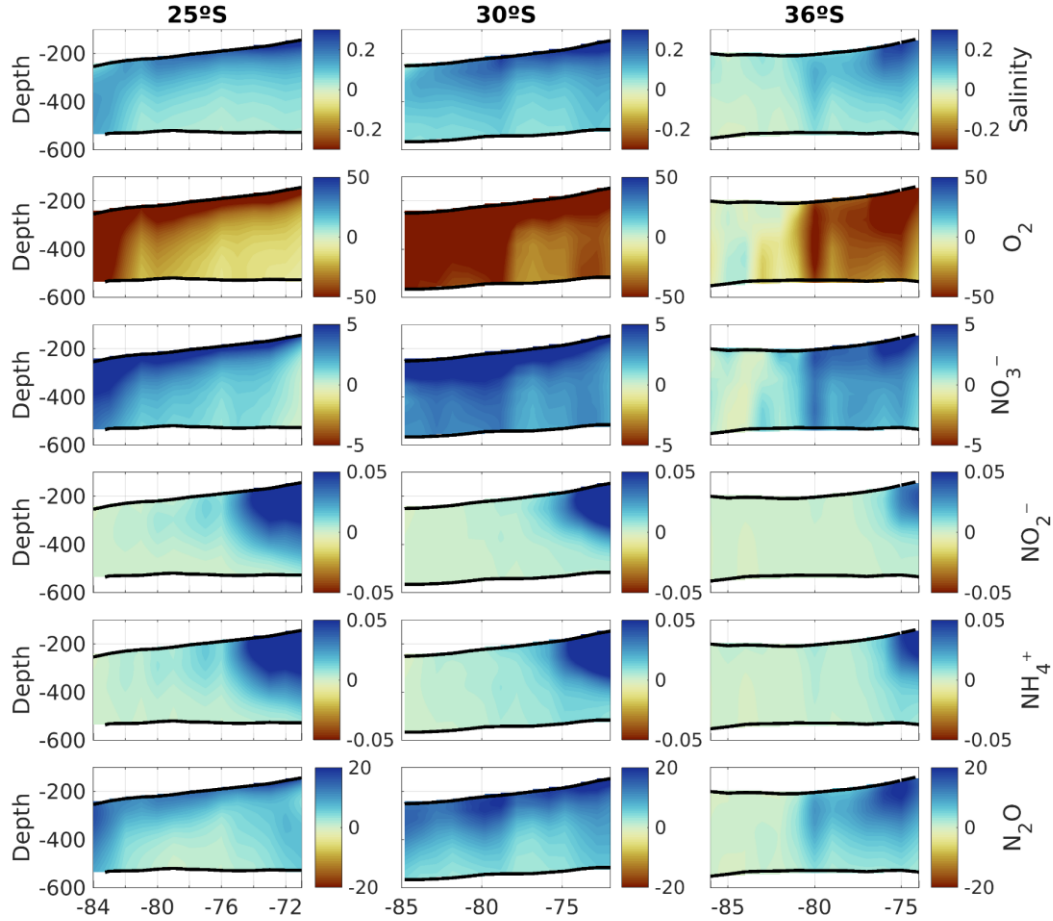
596

597
598 **Figure 9. Puddies composite anomalies for tracers along three zonal bands at different latitudes (25°S - left, 30°S -**
599 **middle and 36°S - right). In order from top to bottom: absolute salinity (g kg^{-1}), oxygen, nitrate, nitrite,**
600 **ammonium (μM) and nitrous oxide (nM). Anomalies are only shown between the isopycnals layers S$_{upper}$ and**
601 **S$_{lower}$ (black contours). The *x*-axis shows the longitude in degrees. The number of Puddies used for the composites**
602 **is identical to that used for Figure 8.**

603

604 Vertical mixing fluxes were positive in newly formed eddies (mainly in coastal regions), while lateral
605 diffusion fluxes showed high variability in magnitude and direction (Figures 7d, 7e).

606

607 **3.4 Subsurface water band changes by Puddies**

608 In this section, a robust approach was used to demonstrate the effect of Puddies on the mean state through the
609 modification of biogeochemical properties, vertical structure, and the contribution of various processes to
610 changes in the subsurface water band delimited by the density surfaces S$_{upper}$ and S$_{lower}$ across different
611 latitudes (25°S, 30°S, and 36°S) during their interaction. All Puddies identified in the three latitudinal bands
612 over the 9-year period were used to build a composite by extracting properties in x-y-z dimensions to obtain
613 the average zonal variables associated with Puddies (details in Section 2.6.2).

22

We compared the characteristics acquired by Puddies in the subsurface band corresponding to 25°S, 30°S, and 36°S with the mean state of the same volume (Figure 8). First, we observed a decrease in salinity farther from the coast, which indicates the intrusion of external waters distinct from the ESSW. At 25°S, Puddies farther from the coast retain saltier water with higher nitrate concentrations (16% higher than mean state) and lower oxygen levels (49% less than mean state) than those at 30°S (12% increase in NO_3^- and 33% decrease in O_2) and 36°S (it finishes completely mixed). Decay rates in Puddies at 30°S are higher than the mean state, except for NO_3^- and N_2O, while at 36°S, only N_2O exhibits a lower decay rate in Puddies (Table 4). At 25°S, the opposite is observed, with lower decay rates in Puddies except for NH_4^+ and NO_3^-. However, the biogeochemical concentrations in both Puddies and the mean state gradually decrease southward. Puddies' contributions are generally higher at 30°S, as shown by anomalies highlighting low O_2 and high NO_3^- and N_2O concentrations (Figure 9). At 25°S, Puddies input more NH_4^+ and NO_2^- (~400% higher than the mean state) in the subsurface band near the coastal zone, while in the oceanic zone, NO_3^- and N_2O (~200% more than the mean state) are the primary contributions, alongside waters with low O_2. The maximum contribution of NO_2^- occurred at 30°S, with a 460% increase compared to the mean state near the coastal zone. At 36°S, Puddies show increased contributions in the transition zones, unlike at other latitudes, with salinity, NO_2^-, and NO_3^- maintaining high concentrations up to 76°W. N_2O also exhibits higher contributions from Puddies at 36°S, particularly in the near-coastal (29% higher than the mean state) and transitional zones. NH_4^+ and NO_2^- concentrations are highest near the formation zones at all three latitudes and decrease sharply in the transitional zones or at the beginning of the oceanic zone. In the northern regions, where the OMZ is broader, and there is less differentiation between water masses, in contrast, farther south, the SAAW erodes the OMZ, making it narrower and causing more abrupt biogeochemical changes between the coastal and transition zones.

Additionally, the dynamics associated with each latitude could drive different changes. The net oxygen budget, referred to as O-RATE in Figure 10, shows that in the upper parts of the eddies, there is always a positive oxygen contribution into the Puddies, with ventilation increasing in the southern eddies within the transitional zone, as seen at 36°S. Oxygen primarily enters through physical processes, with horizontal and vertical advection (HADV and VADV) being dominant (Figure 11). Oxygen depletion in Puddies is also influenced by advective processes, which allow the inflow of less oxygenated waters, ventilating the cores primarily in the middle and lower parts of the eddies (30°S band) or distributed between the S_{upper} and S_{lower} layers in the near-coastal zone (36°S band). Oceanic regions (up to ~800 km offshore) in the 30°S and 36°S bands show intensified SMS activity (e.g., ammonification, zooplankton excretion, and nitrification; Figures 10 and 11). To estimate the time Puddies take to cover a certain distance (i.e., 100 km (~1°)), we could consider a propagation speed of ~2 km/day similar to surface eddies (Chaigneau et al., 2009; Hormazabal et al., 2013). Accordingly, it would take them approximately 50 days to travel that distance. Then, the observed SMS < 0 in the oceanic zone at 30°S remained in the Puddies for about a year.
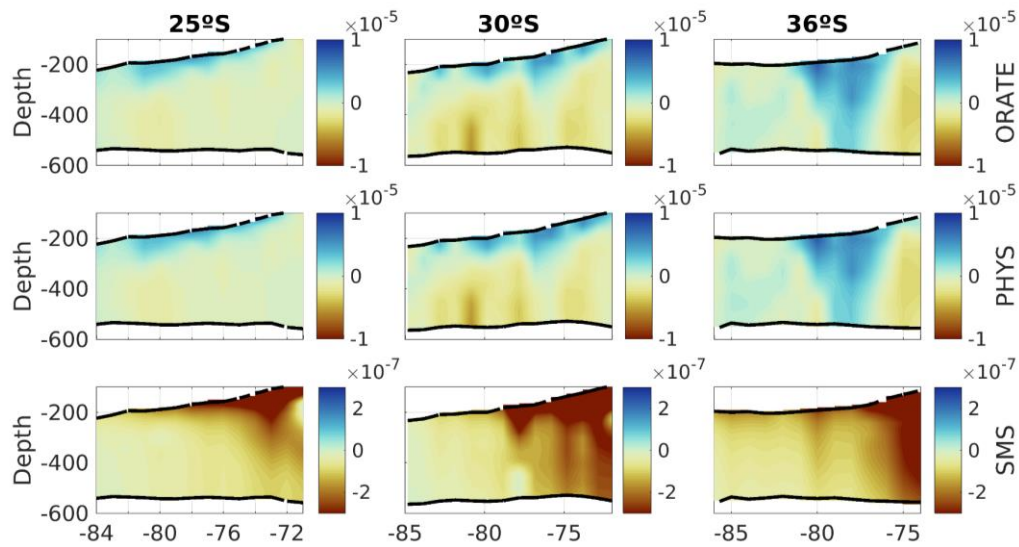
649

650
651 **Figure 10. Same as figure 9 but for the main terms of the O₂ budget: (top panels) the rate of change of oxygen,**
652 **(middle panels) the sum of all physical processes, and (bottom panels) sources minus sinks (SMS) of**
653 **biogeochemical processes.**
654

655 **Table 4. Estimates of the decay rate of tracers along 25°S, 30°S and 36°S for mean state and anomalous conditions**
656 **within Puddies. The decay rate derived from an exponential fit of the form $y = Ae^{-kx}$, where x represents the**
657 **distance from the coast in km and y is the concentration of the biogeochemical tracer. k is the decay rate and A the**
658 **tracer concentration in the coastal strip (1°x1°). A zonal extent of 1,445 km was used at 25°S and 30°S, while at**
659 **36°S we used 1,334 km (i.e. same range of longitude as in Figure 8). Values of k are statistically significant at the**
660 **95% confidence level.**
661

	Decay rate (k) using exponential fit $y = Ae^{-kx}$					
Variable	**Puddies (25ºS)**	**Mean state (25ºS)**	**Puddies (30ºS)**	**Mean state (30ºS)**	**Puddies (36ºS)**	**Mean state (36ºS)**
Salinity	3.35×10^{-6}	3.38×10^{-6}	4.8×10^{-6}	3.5×10^{-6}	5.7×10^{-6}	3.3×10^{-6}
NO₃⁻	4×10^{-5}	1×10^{-4}	1×10^{-4}	1.6×10^{-4}	3.2×10^{-4}	2.6×10^{-4}
NO₂⁻	3×10^{-3}	3×10^{-3}	4×10^{-3}	3×10^{-3}	4×0^{-3}	3×10^{-3}
NH₄⁺	3×10^{-3}	2×10^{-3}	3.1×10^{-3}	2.8×10^{-3}	3×10^{-3}	2×10^{-3}
O₂	-7.6×10^{-4}	-8×10^{-4}	-7.7×10^{-4}	-6×10^{-4}	-7.9×10^{-4}	-5×10^{-4}
N₂O	3×10^{-4}	4×10^{-4}	4×10^{-4}	5×10^{-4}	1×10^{-3}	8×10^{-4}

662

663 At 30°S and 36°S, SMS < 0 extends into the lower parts of the eddies near the coastal zone more intensely

664 (~100 - 150 days), potentially prolonging the lifespan of NO_2^- and NH_4^+. Furthermore, lower oxygen

665 concentrations intrude through HADV and VADV, particularly at 36°S.
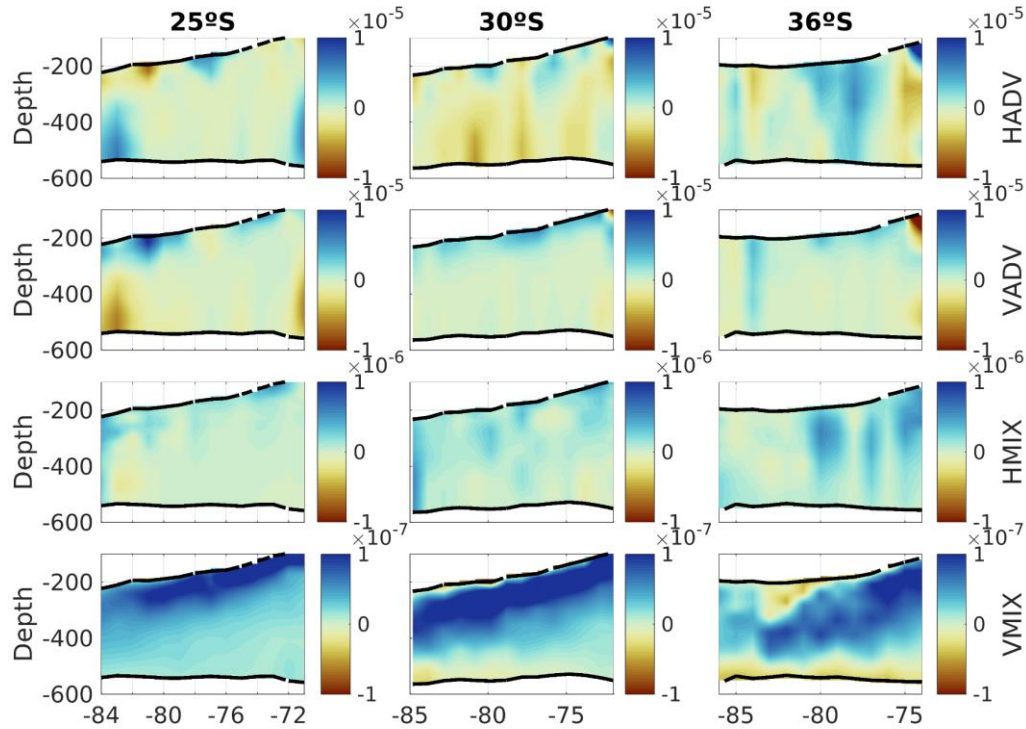
666
667
668

669
670
671 **Figure 11. Same as figure 10 but for the various contributions of PHYS (see Eq. 1). from top to bottom:**
672 **Horizontal advection (HADV), vertical advection (VADV), horizontal mixing (HMIX), vertical mixing (VMIX).**

673 **4 Discussion**

674 Several studies have reported *in situ* subsurface eddies with similar biogeochemical characteristics to those

675 observed in the present study (Stramma et al., 2013; Stramma et al., 2014; Cornejo D'Ottone et al., 2016;

676 Arévalo-Martínez et al., 2016; Grundle et al., 2017; Hormazabal et al., 2013; Kartensen et al., 2017).

677 However, studies focused on a detailed recycling of bioelements within these eddies are scarce. While recent

678 studies have used high-resolution coupled models to describe and quantify more complex processes involved

679 in the O_2, nutrient, or organic matter balance within eddies (José et al., 2017; Frenger et al., 2018; Loveccio

680 et al., 2022), the agents generating natural variability in the lifespan of these bioelements associated with the

681 nitrogen cycle during their trajectory from the OMZ to oceanic waters, have not been analyzed in detail.

682 In this work, a robust statistical analysis was conducted considering all Puddies identified over a 9-year

683 period using two approaches. In the first approach, we characterized the biogeochemical signal of the source

684 water inside the Puddies. Subsequently, we analyzed the eddy cores, focusing on the average Puddies'

685 profiles (using δh_{max}; see Section 2.6.1) and presented the values in the isopycnal layer of 26.6 kg m^{-3} to

assess how and to what extent the biogeochemical properties of the Puddies' cores differ across various regions of the SEP from their formation zone (results in Sections 3.1, 3.2, and 3.3).

In the second approach, we considered the entire volume of the Puddies to characterize their average conditions and quantify how these properties modify the intrathermocline band where the Puddies travel— from the coastal zone, through the transition zone, and into the oceanic zone (see Section 3.4). Additionally, we evaluated the balance of processes involved in the interaction of the Puddies along their trajectory (details in Sections 3.3 and 3.4). This analysis allowed us to identify differences in the impact of Puddies at different latitudes and gain a deeper understanding of the processes involved.

4.1 Biogeochemical anomalies in Puddies from their formation

Subsurface anticyclonic eddies appear to be formed by separating the Peru-Chile Undercurrent from the slope (e.g., Molemaker et al., 2015; Thomsen et al., 2016; Contreras et al., 2019). Here, we observed a higher recurrence of Puddies in specific sectors, namely, between 29°-35°S (Figure 1b), related to the widening of the continental shelf. This change in topography may lead to greater separation of the PCUC from the slope, creating favorable conditions for the generation of Puddies, as observed by Chaigneau et al. (2009). Puddies appear to originate from instabilities forced in the bottom boundary layer at the upper continental slope where the core of the PCUC interacts with the sea bottom (Contreras et al., 2019), and where the core of the OMZ is observed. This water, trapped within the Puddies, is characterized by positive NH_4^+, NO_3^-, NO_2^- and N_2O anomalies and very low O_2 that vary with latitude, as described in Section 3.1. However, unlike O_2 and salinity, which exhibit a more uniform gradient along the coast, several other biogeochemical components have more irregular spatial distributions depending on whether conditions are hypoxic or suboxic.

In the northern part of the coastal zone, limited ventilation creates an environment with suboxic conditions and denitrification, resulting in NO_3^- and N_2O deficits, and NO_2^- and NH_4^+ enrichment. In contrast, the central coastal waters exhibit increased NO_3^-, with the southern part showing higher N_2O concentrations. Additionally, as the formation of Puddies is associated with cross-shore velocities – exchanging nutrients between the continental shelf and open sea (Thompsen et al., 2015) – the mixture of ESSW and SAAW waters, also affected by the southward reduction in the contribution of ESSW (Figure 2; Silva et al., 2009), enhances the biogeochemical variability of the Puddies generated along the Chilean coast (Figure 3).

In summary, Puddies formed along the Chilean coast capture distinct biogeochemical "signatures" depending on where they form. In the north, minimal ventilation fosters suboxic conditions and denitrification –leading to deficits of NO_3^- and N_2O but high NO_2^- and NH_4^+– whereas central and southern subregions show increased NO_3^- and higher N_2O. Moreover, cross-shore exchange between ESSW and SAAW further amplifies this variability, giving rise to eddies with diverse nutrient and oxygen properties as they move offshore.

4.2 Persistence of Biogeochemical Anomalies Away from the Coast

In each subregion (Figure 1a), the Puddies exhibited distinct biogeochemical configurations, as summarized in Figures 4, 5, and 6 (results in Section 3.2). The dominance of SAAW in the southern regions explains the largest number of hypoxic Puddies containing higher O_2 concentrations and lower levels of NO_3^-, NH_4^+, NO_2^-, and N_2O compared to Puddies farther north, where suboxic cores are more prevalent (Silva et al., 2009). Consequently, Puddies that capture a larger fraction of ESSW during their formation exhibit biogeochemical contributions closer to the P75 (Figure 5, Table S2) and show a higher O_2 deficit than the mean state. This suggests that the southern regions are experiencing greater deoxygenation and nutrient enrichment due to the influence of Puddies compared to the northern regions, where the OMZ is much broader.

When estimating the percentage of core distributions exhibiting hypoxia and suboxia, the results showed that hypoxic cores predominantly occur in oceanic waters (Table 2). In general, as we move away from the Chilean coast, biogeochemical element concentrations decrease significantly, though the magnitude of the decrease varies by element (Figure 4). Although Puddies share common characteristics within each region, some variability is observed. This reflects the variety of drivers - such as kinetic and potential energy, vorticity and other dynamics - as well as the differences in the properties of the source water it encloses, its trajectory (potentially interacting with different external water masses), and the physical and biogeochemical processes occurring within it during its lifespan. These factors can enhance or diminish the Puddy's ability to transport properties far from its formation zone.

However, the results indicate an effective transport of these properties to oceanic regions, where values exceed the P90. In contrast, for the transition zones (NTZ and STZ), only AOU, salinity, and NH_4^+ exceed the P90, while ΔN_2O and ΔNO_3^- are closer to the P75. This regional difference clearly demonstrates that the perturbations to the mean state caused by Puddies are more significant in the open ocean than near the coast (Figures 4 and 5; Table S1).

4.3 Changes in the Biogeochemistry of Subsurface Water Masses by the Puddies

Our results showed changes from the coastal to oceanic zones across three latitudes, where a decrease in dissolved inorganic nitrogen compounds, along with a salinity decay rate, confirmed that Puddies age and mix with external waters as they move into the oceanic zone (Figure 8; Table 4). Similar patterns were observed by José et al. (2017) in the upwelling system off Peru, Frenger et al. (2018) across the main EBUS, and Loveccio et al. (2022) in the Northern Canary upwelling system. This offshore change suggests that Puddies have relatively permeable boundaries, but the level of coherence and isolation within the Puddy core can significantly influence the lifespan of compounds enclosed in it. The macronutrient behavior observed was consistent with Frenger et al. (2018), though in our case, N_2O —despite its minimal concentrations— exhibited a pattern similar to other macronutrients, such as NO_3^- (Figure 8). Decay rates for NO_2^- and NH_4^+ were faster than those for NO_3^- and N_2O (Table 4).

756   Nitrate showed higher concentrations compared to other nitrogen compounds. Additionally, as long as NH_4^+

757   and NO_2^- are present (Figures 4, 8, and 9), nitrification can replenish the NO_3^- pool in subsurface waters

758   where photosynthesis does not consume it. In addition, N_2O production depends on $[NH_4^+]$, $[NO_2^-]$, and $[O_2]$

759   levels and the nitrification and denitrification processes. According to the model parameterization (for more

760   details, see Gutknecht et al., 2013a), the maximum N_2O production occurs when $O_2 = 1$ μM, with $SMS(N_2O)$

761     $= \alpha(\text{Nitrif}) + \beta(\text{Nitrif})$ (α, β constant), whereas when O_2 is high or $O_2 < 1$ μM, the N_2O production decreased

762   because $SMS(N_2O) \rightarrow \alpha(\text{Nitrif})$. On one hand, N_2O production diminishes as NO_2^- and NH_4^+ availability

763   declines, as observed in the open sea; on the other hand, in coastal zones, denitrification rapidly depletes

764   these compounds until N_2O production ceases at oxygen concentrations below 1 μM. Since the model does

765   not account for N_2O consumption by biological processes (via denitrification or fixation) but only through

766   atmospheric exchange, the Puddies act as a source of N_2O as they move offshore and the observed N_2O

767   decrease within Puddies can only result from physical processes facilitating exchange with external waters.

768   Notably, the 30°S zonal band exhibited the largest anomalies in biogeochemical characteristics (Figure 9).

769   Along this band, the high occurrence of Puddies, including those formed at or south of this latitude, is

770   significant due to the characteristic northwest trajectory of eddies. This could explain the high nutrient

771   concentrations there (Figure 3). Newly formed Puddies must be supported by dissolved organic nitrogen

772   from the source water with higher O_2 consumption (*SMS*) during the first 100-150 days, as Loveccio et al.

773   (2022) proposed. Mixing with external waters (Figure 8) is driven by physical processes, particularly

774   advection (HADV and VADV, Figures 10 and 11). Compared to the other two latitudes, higher O_2

775   consumption (SMS < 0) at 30°S suggests higher local nutrient production through remineralization (i.e.,

776   more organic material is being broken down), potentially extending the lifespan of NO_2^- and NH_4^+, necessary

777   for the ΔN_2O and ΔNO_3^-, activity that remained in the Puddies for about a year around 800 km offshore.

778   Biological activity sustains low-oxygen cores for longer periods, preserving original conditions even with O_2

779   < 20 μM in the cores, where denitrification continues while the edges ventilate. Additionally, horizontal

780   advective processes further reduce oxygen levels in the lower part of the eddy by allowing the intrusion of

781   low-oxygen waters, contrasting with observations at 25°S and 36°S.

782   This combination of conditions suggests that regions of significant interaction with Puddies can transform the

783   biogeochemistry of the subsurface layer in meaningful ways. Both approaches used to characterize Puddies

784   provide valuable insights into how and to what extent these Puddies evolve, driving changes in the

785   intrathermocline from their formation to their dispersion across the SEP.

786   **4.4 Advantages and Disadvantages of the Model for Low Oxygen Conditions**

787   We now discuss the limitations of the model formulation in accounting for the transition between the two

788   oxygen regimes (hypoxic versus suboxic) and its implication for Puddies life cycle. AOU:NO_3^- ratios of

789   250:30 (up to 20:1) have been documented in the Atlantic from *in situ* monitoring of NO_3^- within mode water

790   eddies (Kartensen et al., 2017) and in eddy cores with $NO_3^- < 25$ μM at $O_2 < 5$ μM in the SEP (Stramma et

791   al., 2013). The eddies modeled here showed AOU values similar to those found by Karstensen et al. (2017)

792   in the eastern tropical North Atlantic, although NO_3^- was overestimated by 3 - 5 μM leading to an

793 AOU:ΔNO_3^- ratio of 5:1 (Figures 4b and 6 - upper box; Stramma et al., 2013). Suboxic Puddies build up

794 NO_2^-, although the modeled maximum concentration appears underestimated compared to previously

795 reported *in situ* data (Stramma et al., 2013; Cornejo et al., 2012; Cornejo-D'Ottone et al., 2016).

796 Consequently, the relationship between NO_2^- and ΔN_2O in the northern zone also showed underestimation.

797 At the modeled N_2O maximum (>30 nM, Figure 6), field data shows NO_2^- values >1 μM (Cornejo et al.,

798 2012), while the modeled NO_2^- maximum reaches 0.15 μM (Figures 4 and 5). Comparing our results with

799 eddies monitored in the SEP, the N_2O concentrations observed in open ocean eddies agree with those

800 measured by Cornejo-D'Otonne et al. (2016; Figure 4d, S5) in an eddy originated near the coast off

801 Concepcion (~37°S, south zone), although there are differences of up to 20 nM with the eddy reported by

802 Arévalo-Martínez et al. (2016; Figure 4d, S5) off northern Chile. These results suggest a better representation

803 of biogeochemical processes by the model in a hypoxic than suboxic environment.

804 Biogeochemical components are challenging to model due to the numerous physical, biogeochemical, and

805 biological processes involved. Specifically, under hypoxic or suboxic conditions, the nitrogen cycle is more

806 complex due to additional processes that occur within a narrow O_2 range, increasing the system's sensitivity.

807 Processes removing nitrogen from the system, such as denitrification, also generate intermediate products

808 such as N_2O and NO_2^- (e.g., denitrification, NO_3^- reduction). Denitrification is a complex process to

809 parameterize, involving a range of steps for each nitrogen component and various rates of decomposition of

810 particulate (large and small) and dissolved material. However, despite the attempt to consider these processes

811 realistically, the model remains an approximation but reasonably represents the involved processes, primarily

812 within the intrathermocline band (see Appendix). In the suboxic zone, while the model underestimated O_2,

813 NO_3^- remained overestimated, but in the subsurface band associated with the OMZ core, the model

814 represented the lowest biases in O_2 and nitrogen evaluated with climatological observations (see Appendix).

815 This allowed us to present a robust statistical analysis of biogeochemical properties inside and outside the

816 Puddies. Despite the difficulty in simulating realistically sharp mean gradients in water mass properties

817 (Pizarro-Koth et al., 2019), the model did highlight typical features, such as NO_3^- consumption and

818 production of NO_2^- and N_2O, processes that persist within Puddies far from their origin within the OMZ.

819

820 **5 Conclusions**

821 Using a high-resolution coupled simulation of the SEP, we characterized the biogeochemical changes within

822 Puddies, their differences with the external properties, and the processes involved in the O_2 balance during

823 their transport to oceanic waters. The model resolved eddy dynamics and biogeochemical processes related to

824 the nitrogen cycle, including characteristic EBUS processes such as denitrification. This methodology

825 allowed us to statistically approximate the biogeochemical changes occurring within these Puddies, quantify

826 the modifications to water bodies along their paths, and identify the dominant mechanisms regulating

827 compound concentrations from the formation zone to hundreds of kilometers offshore.

828 During formation, Puddies capture a biogeochemical signal that varies depending on their origin, which is

829 associated with the core of the Peru-Chile Undercurrent. Peripheral permeability enables exchange with

830 external waters, modulating the original signature. However, the core signal retains characteristic negative O_2

831 anomalies and positive anomalies for other biogeochemical tracers. These disturbances may cause average

832 properties to exceed the 90th percentile (P90) in the open ocean, in contrast to the formation zone, where

833 values remain above the 50th percentile (P50). While a high percentage of Puddies near the coast exhibit

834 suboxic cores (all in the north and 70% in central-south Chile), the proportion decreases with distance from

835 the coast, where hypoxic cores become predominant (60% in the STZ and NOZ). This suggests core

836 ventilation during their trajectory, as indicated by an estimate of the salinity decay rate as a function of

837 latitude.

838 The dominant mechanism for O_2 exchange in the eddy core is lateral and vertical advection, with vertical

839 mixing contributing two orders of magnitude less. O_2 consumption through biological activity (SMS) was

840 maintained inside the Puddies (around 6 to 12 months) up to the oceanic zones (e.g., at 30°S the O_2

841 consumption was maintained up to ~800 km from the coast), enabling the persistence of low O_2 conditions

842 in the core despite peripheral ventilation. This persistence supports processes such as denitrification, which

843 occur under hypoxic or suboxic conditions within the OMZ, and can extend into areas far beyond the OMZ,

844 sustained in core niches with $O_2 < 20$ μM. The SCZ and STZ experience significant deoxygenation and

845 nutrient enrichment due to Puddies formed with larger anomalies. At 30°S, a combination of factors

846 significantly impacts the intrathermocline biogeochemistry due to Puddies transiting this latitude. The

847 maximum contribution of NO_2^- occurred at 30ºS, with a 460% increase compared to the mean state, near the

848 coastal zone. Clearly, the formation of Puddies is a critical process in extending the OMZ boundaries at its

849 southern edge. Additionally, the interplay of physical conditions can generate regions with substantial

850 subsurface water mass changes due to interactions with Puddies.

851 Biogeochemical tracers exhibit varying lifespans depending on their original concentrations, as well as their

852 demand and production rates. Ammonium (NH_4^+) and nitrite (NO_2^-) tend to decline first, whose

853 concentration was maximum in the coastal zone (300-400% higher than mean state), with high decay rates

854 with distance from the coast, while other components decrease more slowly and persist longer. Despite being

855 produced in low concentrations, N_2O is retained in Puddies farther from the coast, serving as a proxy for

856 denitrification in the source water and contributing to the subsurface reservoir of this greenhouse gas in the

857 open ocean (up to ~100% higher than the mean state). Characterizing Puddies provides valuable insights into

858 how they evolve and drive intrathermocline changes from their formation to dispersion across the SEP.

859 Beyond offering insights into the biogeochemical dynamics of Puddies, this study's findings can also help

860 guide *in situ* monitoring, particularly in remote areas where unusual biogeochemical signals may indicate the

861 presence of a Puddy.

862 Higher-resolution models enable better characterization of mixing processes involved in eddy core

863 ventilation and the exchange of properties with external waters through submesoscale dynamics (Brannigan

864 et al. 2017). Coupling with more complex biogeochemical models will help quantify the effects of additional

865 SMS processes within Puddies not included in this study. This is planned for future research. Validation and

866 supplementary statistics through further observations in the study area are also recommended to deepen our

867 understanding of coupled processes in surface and subsurface eddies.

868

Appendix: model assessment

A.1 Data

Observed climatological O_2 and NO_3^- fields were taken from the CSIRO Atlas of Regional Seas (CARS2009; www.marine.csiro.au/~dunn/cars2009/) for the biogeochemical model assessment, which has a spatial resolution of 0.5 degrees and a monthly mean resolution. The model validation was performed over the first 800 m. The vertical resolution of the data set is 10 meters to the first 300 m, 25 meters to 500 m, and 50 meters down to 800m.

A.2 Surface Nitrate

The model simulates low NO_3^- (< 2 μM) in general, except in the areas near the coast and in the southwest where concentrations reached 8 μM (Fig. A1a). The observed concentrations were higher, particularly in the south (Fig. A1b). Overall, the model underestimated NO_3^- concentrations in most of the domain, although the differences with observations remain relatively small, ranging between 0 - 4 μM south of 30ºS and between 0-2 μM north of 30ºS (Figs. A1a, A1c). Adjacent to the coast between 25º-35ºS, the model overestimates concentrations by ~7 μM (Fig. A1c). In general, differences were minimal over most of the study area, and it can therefore be considered that the model fairly well represents surface NO_3^-.
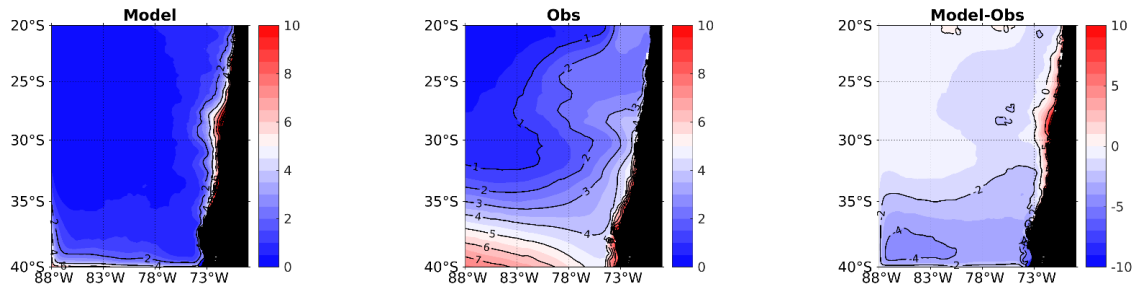
Figure A1. Spatial distribution of mean surface NO_3^-. (a) ROMS-BioEBUS simulation, (b) CARS climatology, and (c) BIAS (model - observations). Units are μM.

A.3 Oxygen and nitrate on the isopycnal layers

The comparison between observations and model is here done over different density layers S_{upper}, S_{lower} and S_{core} (Figures A2, A3, A4). The model captures the principal characteristics of O_2 and NO_3^-, displaying a similar structure and latitudinal and zonal gradients. Compared with observed data, lower O_2 concentrations and higher NO_3^- concentrations were predicted near the coast and north of 30ºS associated with the meridional changes of the offshore extension of the OMZ.

31

895   In the S_{upper} surface, observations reveal discontinuous areas with lower O_2 concentrations north of 25ºS (O_2

896   <100 μM), between 30 - 31ºS and 35 - 36ºS (O_2 <150 μM). The model mostly underestimated these O_2

897   concentrations by 40 μM north of 30ºS, by around 20 μM between 30 - 35ºS, and overestimated them by 20

898   μM between 35 - 38ºS near the slope, but performed better south of 35º S offshore. For NO_3^-, observations

899   indicated very low concentrations mainly along the coast between 23 - 35ºS (<10 μM), with an increase

900   to >15 μM in the oceanic region. Therefore, the model overestimated concentrations in the coastal zone (>10

901   μM) and in the northern oceanic zone (4 - 8 μM, Figures A2).

902   Regarding the S_{core} layer, the model performed better in the northern region, underestimating O_2

903   concentrations between 0 - 10 μM. Off the coast, the bias ranged from -10 to 10 μM. However, south of 30º

904   S, between 75 - 80ºW, the model overestimated O_2 concentrations by over 40 μM, whereas west of 82ºW, the

905   bias varied between -10 to 10 μM. Nitrate concentration is overestimated by the model in the coastal region

906   with concentrations exceeding 6 - 8 μM, particularly in the northern oceanic area (2 - 4 μM). The model is

907   more realistic in terms of NO_3^- in the region west of 78ºW and south of 30ºS (Figure A3).

908
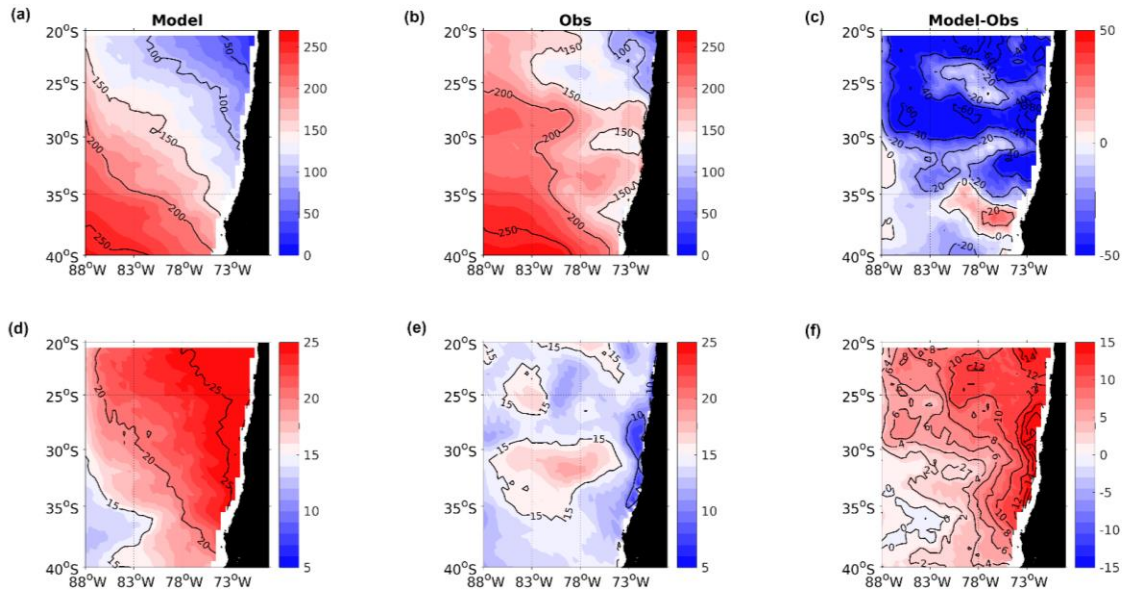
909   **Figure A2. (top panels, a-c) Mean O_2 and (bottom panels, d - f) mean NO_3^- concentration in the isopycnal layer**

910   **S_{upper} = 26.0 kg m^{-3} from the ROMS-BioEBUS simulation (left), the CARS climatology (middle), and the BIAS**

911   **(right). Units are μM..**

912
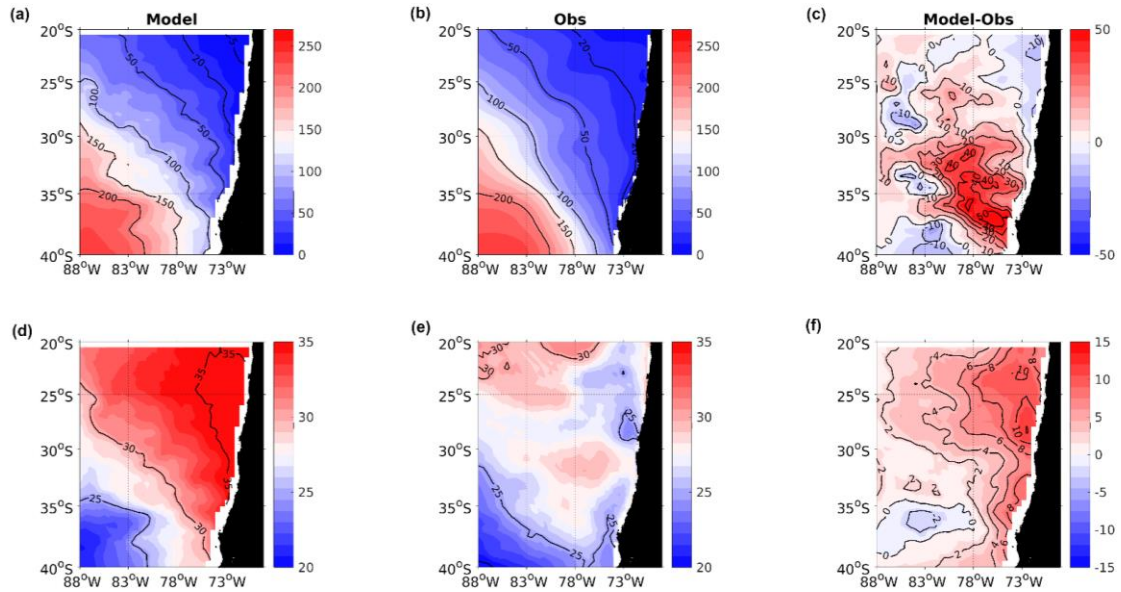
913   **Figure A3. Same as Figure A2 but for the isopycnal layer S_core = 26.6 kg m⁻³.**

914
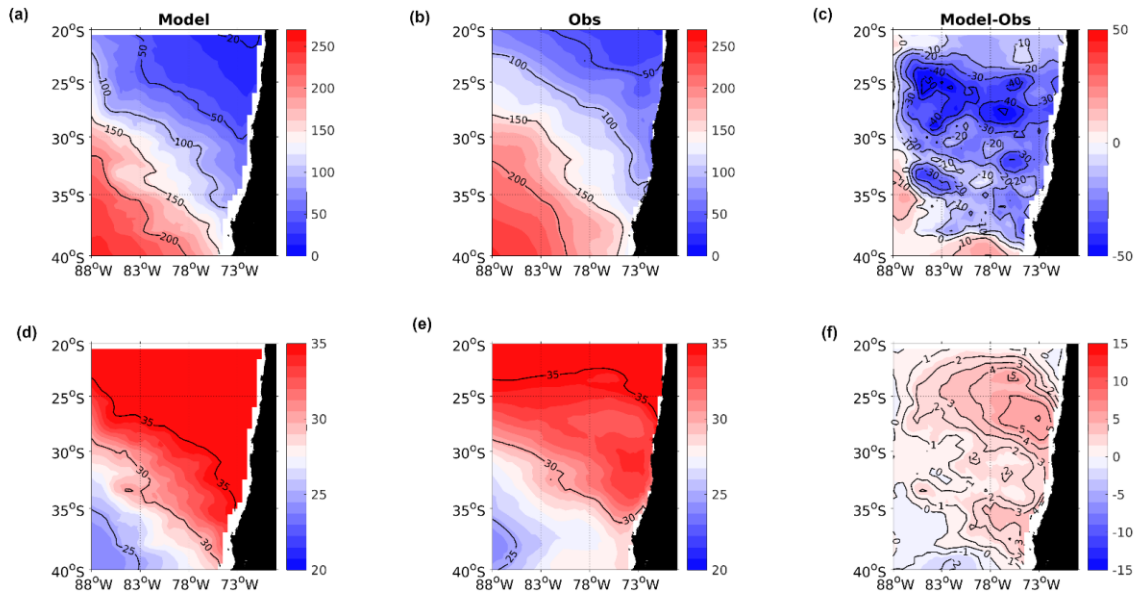
915   **Figure A4. Same as Figure A2 but for the isopycnal layer S_lower = 26.9 kg m⁻³.**

916   In the S_{lower} layer, the model simulates in general lower O_2 concentrations than observations north of 30ºS ,

917   underestimating by between 10 - 40 µM. This bias is smaller south of 30º S (10 - 30 µM) and in the

918   southwest (0 - 10 µM). The model realistically simulates NO_3^-, with deviations from observations ranging

919   from -2 to 5 µM and with the greatest overestimation occurring in the region where $O_2 < 50$ µM (Figure A4).

920

921   **A.4 Vertical Structure**

The comparison between model and observations is done along zonal sections at 25ºS, 30ºS, and 35ºS (Figures A5, A6). Along the latitudinal gradient, the contour of 50 μM shows that the OMZ narrows towards the south. Observations evidence an elongated low-oxygen tongue in subsurface waters that is more pronounced than in the model simulations, along with an intrusion of oxygenated waters both at the surface and at depth (~600 m), enclosing the low-oxygen water with a marked oxycline (Figure A5). The oxyclines showed a greater bias, with the model tending to underestimate the observed data, particularly in the lower oxycline with an underestimation of up to 60 μM. In the subsurface layer between 200 - 400 m, the model better represents O_2 levels, especially at 25 - 30ºS where differences ranged from 0 - 10 μM (Figure A5c, A5f). At 35ºS, there is an overestimation (40 μM) between 75-80ºW low 200 - 300 m depth (Figure A5i).
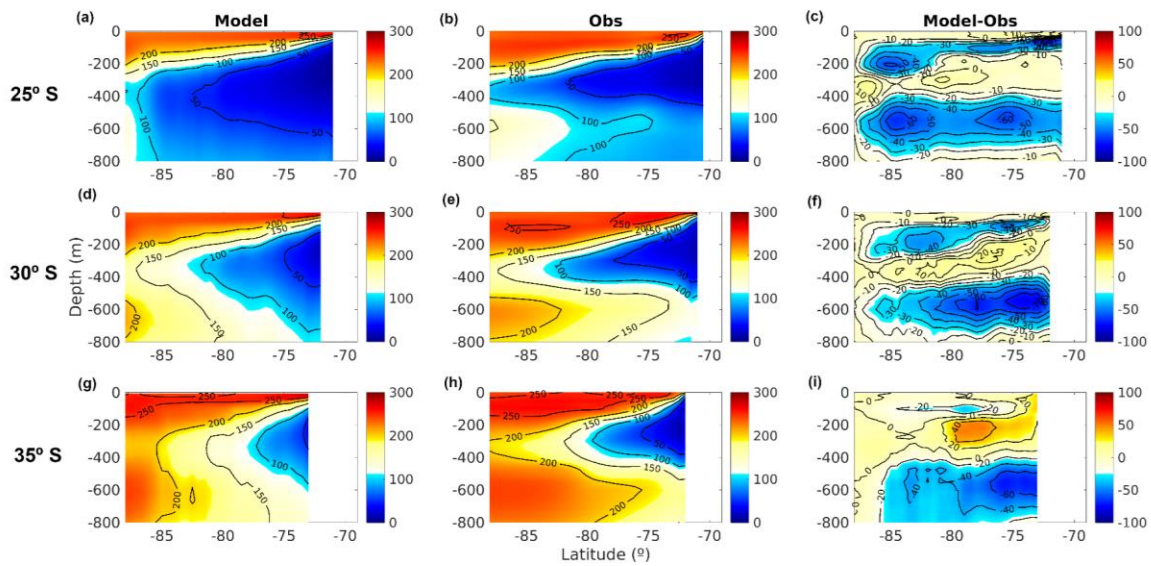
Figure A5. Zonal section of mean O_2 concentration at (a - c) 25ºS, (d - e) 30ºS, and (f - h) 35ºS. (a, d, g) from the ROMS-BioEBUS simulation (left boxes), CARS climatology (middle boxes), and BIAS (right boxes). Units are μM.

Along 25ºS the model simulates higher subsurface NO_3^- concentrations near the coast compared to observations, showing differences of up to 15 μM. Below 400 m of depth, overestimations range from 0 - 4 μM (Figure A6a, A6b, A6c). These differences decrease towards the south; at 30ºS and 35ºS, the most significant differences extend from the coast to 76ºW and below -300 m (overestimations of 8 - 12 μM), whereas elsewhere, the differences remain between 0 - 4 μM. Subsurface NO_3^- is underestimated by 2 μM by the model at 35ºW and west of 80ºW (Figures A6f, A6i).

Taylor diagrams synthesize the agreement between model and observations for the annual mean O_2 and NO_3^- in each of the subregions integrated in the upper 800 m of the water column (Figures A7, A8). Estimates of standard deviation, correlation, and RMSE reveal that the current model configuration is generally in reasonable agreement with observations, primarily in the subsurface layer where most of the properties of Puddies were computed (Figure A9). Therefore, there is confidence in using the model for the biogeochemical characterization of these mesoscale processes.

947
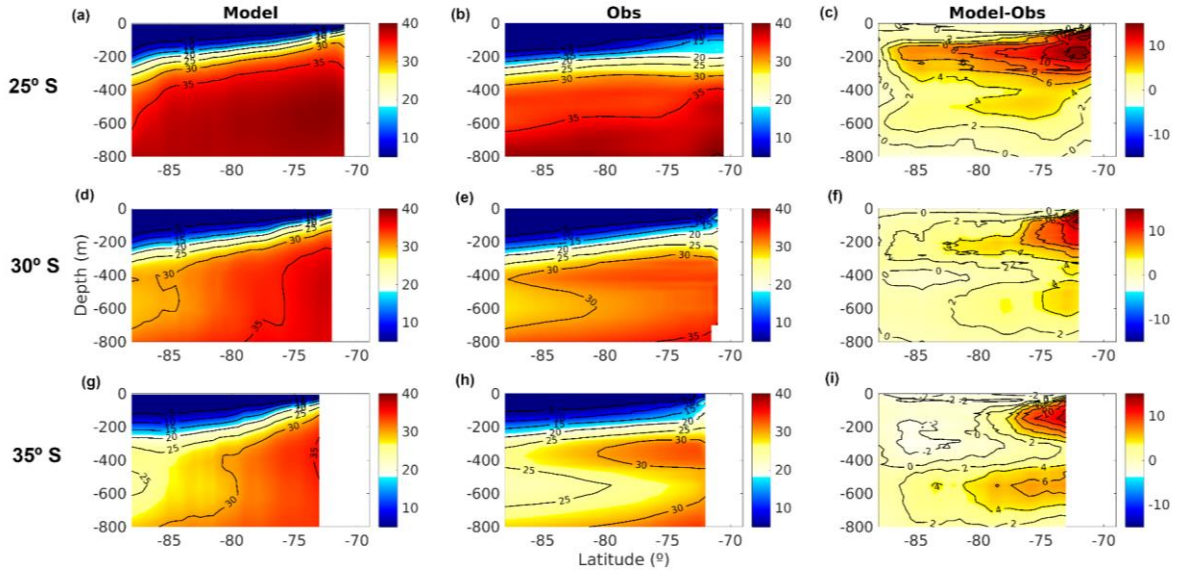
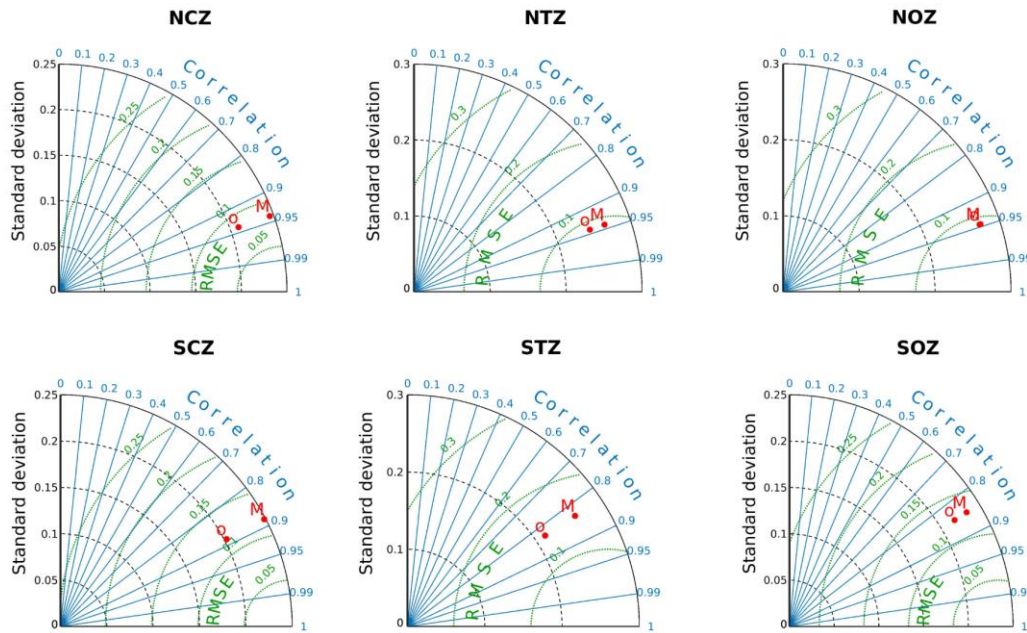**Figure A6. Same as Figure A5 but for mean NO₃⁻ concentration.**

949

950

Figure A7. Taylor diagram for mean O₂ concentrations over the six subregions (Figure 1a) and within the first 800m. M is for the model while O is for the CARS climatology. The X-Y axis refers to the standard deviation (black lines), correlations in the radial axis (blue lines) and RMSE is indicated by curved lines (green). Region's names are: Northern Coastal Zone (NCZ); Northern Transition Zone (NTZ); Northern Oceanic Zone (NOZ); Southern Oceanic Zone (SOZ); Southern Transition Zone (STZ) and Southern Coastal Zone (SCZ).

956

957
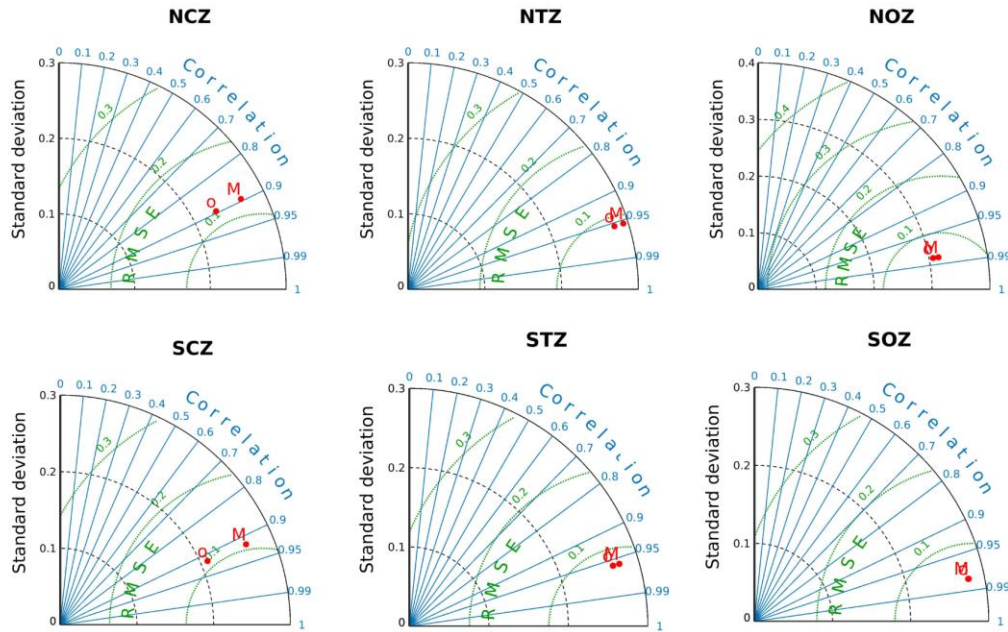
Figure A8. Same as figure A7 but for mean NO₃⁻ concentration.

959
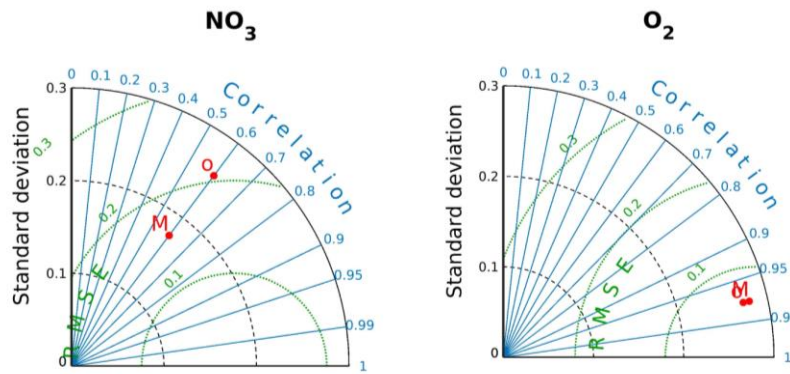
Figure A9. Taylor diagram for mean NO₃⁻ and O₂ concentrations over the entire S$_{core}$ volume. Details are similar to those in Figures A7 and A8.

Code availability

ROMS model code is available at http://www.croco-ocean.org. All input data set and configuration of our ROMS/BIOEBUS simulations are described in section and in the references therein. This work was granted access to the HPC resources of CALMIP supercomputing center at the Toulouse University under the allocations 2023-1044 and 2024-1044.

Author contributions

36

968 LOC, OP, MC and BD designed the study. BD performed the simulation. LOC made the assessment, eddy
969 identification and statistical analysis of the model outputs. OP supervised the project. LOC interpreted the
970 results and wrote the manuscript with contributions from all co-authors.

981 **References**
982
983 Almendra, I., Dewitte, B., Garçon, V. et al.: Emergent constraint on oxygenation of the upper South Eastern
984 Pacific oxygen minimum zone in the twenty-first century, Commun Earth Environ, 5, 284,
985 https://doi.org/10.1038/s43247-024-01427-2, 2024.

986 Altabet, M. A., Ryabenko, E., Stramma, L., Wallace, D. W., Frank, M., Grasse, P., and Lavik, G.: An eddy-
987 stimulated hotspot for fixed nitrogen-loss from the Peru oxygen minimum zone, Biogeosciences, 9(12),
988 4897-4908, https://doi.org/10.5194/bg-9-4897-2012, 2012.

989 Arévalo-Martínez, Damian L., Annette Kock, Carolin R. Löscher, Ruth A. Schmitz, Lothar Stramma, and
990 Hermann W. Bange.: Influence of Mesoscale Eddies on the Distribution of Nitrous Oxide in the Eastern
991 Tropical South Pacific, Biogeosciences 13 (4): 1105–18, https://doi.org/10.5194/bg-13-1105-2016, 2016.

992 Auger, P. A., Bento, J. P., Hormazabal, S., Morales, C. E., and Bustamante, A.: Mesoscale variability in the
993 boundaries of the oxygen minimum zone in the eastern South Pacific: Influence of intrathermocline eddies,
994 Journal of Geophysical Research: Oceans, 126, e2019JC015272, https:// doi.org/10.1029/2019JC015272,
995 2021.

996 Bettencourt, J. H., López, C., Hernández-García, E., … and Garçon V.: Boundaries of the Peruvian oxygen
997 minimum zone shaped by coherent mesoscale dynamics, Nature Geoscience, 8(12), 937–940,
998 https://doi.org/10.1038/ngeo2570, 2015.

999 Brannigan, L., Marshall, D. P., Naveira, A. C., George, A. J., Kaiser, J.: Submesoscale instabilities in
1000 mesoscale eddies, J. Phys. Oceanogr., 47, 3061-3085, https://doi.org/10.1175/JPO-D-16-0178.1, 2017.

1001 Calil, P. H. R.: High-resolution, basin-scale simulations reveal the impact of intermediate zonal jets on the
1002 Atlantic oxygen minimum zones. Journal of Advances in Modeling Earth Systems, 15, e2022MS003158,
1003 https://doi.org/10.1029/2022MS003158, 2023.

1004 Chaigneau, A., Eldin, G., and Dewitte, B.: Eddy activity in the four major upwelling systems from satellite
1005 altimetry (1992–2007), Progress in Oceanography, 83(1-4), 117-123,
1006 https://doi.org/10.1016/j.pocean.2009.07.012, 2009.

1007 Chaigneau, A., Le Texier, M., Eldin, G., Grados, C., and Pizarro, O.: Vertical structure of mesoscale eddies
1008 in the eastern South Pacific Ocean: A composite analysis from altimetry and Argo profiling floats, Journal of
1009 Geophysical Research, 116(C11), C11025, https://doi. org/10.1029/2011JC007134, 2011.

1010 Chenillat, F., Franks, P. J., and Combes, V.: Biogeochemical properties of eddies in the California Current
1011 System. Geophysical Research Letters, 43(11), 5812-5820, https://doi.org/10.1002/2016GL068945, 2016.

1012 Collins, C. A., Margolina, T., Rago, T. A., and Ivanov, L.: Looping RAFOS floats in the California current
1013 system, Deep Sea Research Part II: Topical Studies in Oceanography, 85, 42-61,
1014 https://doi.org/10.1016/j.dsr2.2012.07.027, 2013.

1015 Combes, V., Hormazabal, S., and Di Lorenzo, E.: Interannual variability of the subsurface eddy field in the
1016 Southeast Pacific, Journal of Geophysical Research: Oceans, 120(7), 4907-4924,
1017 https://doi.org/10.1002/2014JC010265, 2015.

1018 Contreras, M., Pizarro, O., Dewitte, B., Sepulveda, H. H., and Renault, L.: Subsurface mesoscale eddy
1019 generation in the ocean off central Chile, Journal of Geophysical Research: Oceans,
1020 https://doi.org/10.1029/2018JC014723, 2019

1021 Cornejo D'Ottone, M., Bravo, L., Ramos, M., Pizarro, O., Karstensen, J., Gallegos, M., Correa-Ramirez, M.,
1022 Silva, N., Farias, L., and Karp-Boss, L.: Biogeochemical characteristics of a long-lived anticyclonic eddy in
1023 the eastern South Pacific Ocean, Biogeosciences, 13, 2971–2979, https://doi.org/10.5194/bg-13-2971-2016,
1024 2016.

1025 Couespel, D., Lévy, M., and Bopp, L.: Major contribution of reduced upper ocean oxygen mixing to global
1026 ocean deoxygenation in an Earth system model, Geophysical Research Letters, 46(21), 12239–12249,
1027 https://doi.org/10.1029/2019GL084162, 2019.

1028 Czeschel, R., L. Stramma, R. A. Weller, and T. Fischer.: Circulation, Eddies, Oxygen, and Nutrient Changes
1029 in the Eastern Tropical South Pacific Ocean, Ocean Science 11 (3): 455–70, https://doi.org/10.5194/os-11-
1030 455-2015, 2015.

1031 Dadou, I., Lamy, F., Rabouille, C., Ruiz-Pino, D., Andersen, V., Bianchi, M., and Garçon, V.: An integrated
1032 biological pump model from the euphotic zone to the sediment: a 1-D application in the Northeast tropical
1033 Atlantic, Deep Sea Research Part II: Topical Studies in Oceanography, 48(10), 2345-2381,
1034 https://doi.org/10.1016/S0967-0645(00)00177-6, 2001.

1035 Dadou, I., G. Evans, and V. Garçon.: Using JGOFS in situ and ocean color data to compare biogeochemical
1036 models and estimate their parameters in the subtropical North Atlantic Ocean, Journal of Marine Research,
1037 62, (4), https://elischolar.library.yale.edu/journal_of_marine_research/54, 2004.

1038 Dewitte, B., Vazquez-Cuervo, J., Goubanova, K., Illig, S., Takahashi, K., Cambon, G., ... and Ortlieb, L.:
1039 Change in El Niño flavours over 1958–2008: Implications for the long-term trend of the upwelling off
1040 Peru, Deep Sea Research Part II: Topical Studies in Oceanography, 77, 143-156,
1041 https://doi.org/10.1016/j.dsr2.2012.04.011, 2012.

1042 Dugan, J. P., R. P. Mied, P. C. Mignerey, and A. F. Schuetz.: Compact, Intrathermocline Eddies in the
1043 Sargasso Sea, Journal of Geophysical Research 87 (C1): 385–93, https://doi.org/10.1029/JC087iC01p00385,
1044 1982.

1045 Faghmous, J. H., Frenger, I., Yao, Y., Warmka, R., Lindell, A., and Kumar, V.: A daily global mesoscale
1046 ocean eddy dataset from satellite altimetry, Scientific data, 2(1), 1-16, http://doi.org/10.1038/sdata.2015.28,
1047 2015.

1048 Fauzi, R., Mantoura, C., Law, C. S., Owens, N. J., Burkill, P. H., Woodward, E. M. S., ... and Llewellyn, C.
1049 A.: Nitrogen biogeochemical cycling in the northwestern Indian Ocean, Deep Sea Research Part II: Topical
1050 Studies in Oceanography, 40(3), 651-671, https://doi.org/10.1016/0967-0645(93)90050-W, 1993.

Frenger, Ivy, Daniele Bianchi, Carolin Stührenberg, Andreas Oschlies, John Dunne, Curtis Deutsch, Eric Galbraith, and Florian Schütte.: Biogeochemical Role of Subsurface Coherent Eddies in the Ocean: Tracer Cannonballs, Hypoxic Storms, and Microbial Stewpots?, Global Biogeochemical Cycles 32 (2): 226–49, https://doi.org/10.1002/2017GB005743, 2018.

Garcia, H. E., and Gordon, L. I.: Oxygen solubility in seawater: Better fitting equations, Limnology and oceanography, 37(6), 1307-1312, https://doi.org/10.4319/lo.1992.37.6.1307, 1992.

Goreau, T. J., Kaplan, W. A., Wofsy, S. C., McElroy, M. B., Valois, F. W., and Watson, S. W.: Production of NO_2^- and N_2O by nitrifying bacteria at reduced concentrations of oxygen, Applied and environmental microbiology, 40(3), 526-532, https://doi.org/10.1128/aem.40.3.526-532.1980, 1980.

Goubanova, K., Echevin, V., Dewitte, B., Codron, F., Takahashi, K., Terray, P., and Vrac, M.: Statistical downscaling of sea-surface wind over the Peru–Chile upwelling region: diagnosing the impact of climate change from the IPSL-CM4 model, Climate Dynamics, 36, 1365-1378, https://doi.org/10.1007/s00382-010-0824-0, 2011.

Grados, D., Bertrand, A., Colas, F., Echevin, V., Chaigneau, A., … and Fablet R.: Spatial and seasonal patterns of fine-scale to mesoscale upper ocean dynamics in an Eastern Boundary Current System, Progress in Oceanography, 142, 105–116, https://doi. org/10.1016/j.pocean.2016.02.002, 2016.

Grundle, D. S., C. R. Löscher, G. Krahmann, M. A. Altabet, H. W. Bange, J. Karstensen, A. Körtzinger, and B. Fiedler.: Low Oxygen Eddies in the Eastern Tropical North Atlantic: Implications for N_2O Cycling, Scientific Reports 7 (1): 1–10, https://doi.org/10.1038/s41598-017-04745-y, 2017.

Gutknecht, E., Dadou, I., Le Vu, B., Cambon, G., Sudre, J., Garçon, V., E. Machu, T. Rixen, A. Kock, A. Flohr, and Paulmier, A.: Coupled physical/biogeochemical modeling including O2-dependent processes in the Eastern Boundary Upwelling Systems: application in the Benguela, Biogeosciences, 10(6), 3559-3591, https://doi.org/10.5194/bg-10-3559-2013, 2013a.

Helly, J. J., and Levin, L. A.: Global distribution of naturally occurring marine hypoxia on continental margins, Deep Sea Research Part I: Oceanographic Research Papers, 51, 1159–1168, https://doi.org/10.1016/j.dsr.2004.03.009, 2004.

Hormazabal, Samuel.: Coastal Transition Zone off Chile. Journal of Geophysical Research 109 (C1): C01021, https://doi.org/10.1029/2003JC001956, 2004.

Hormazabal, Samuel, Vincent Combes, Carmen E. Morales, Marco A. Correa-Ramirez, Emmanuel Di Lorenzo, and Sergio Nuñez.: Intrathermocline Eddies in the Coastal Transition Zone off Central Chile (31-41°S), Journal of Geophysical Research: Oceans 118 (10): 4811–21, https://doi.org/10.1002/jgrc.20337, 2013.

Huret, M., Dadou, I., Dumas, F., Lazure, P., and Garçon, V.: Coupling physical and biogeochemical processes in the Rio de la Plata plume, Continental Shelf Research, 25(5-6), 629-653, https://doi.org/10.1016/j.csr.2004.10.003, 2005.

Johnson, G. C., and McTaggart, K. E.: Equatorial Pacific 13 C water eddies in the eastern subtropical South Pacific Ocean, Journal of Physical Oceanography, 40(1), 226-236, https://doi.org/10.1175/2009JPO4287.1, 2010.

Jose, Y. S., Aumont, O., Machu, E., Penven, P., Moloney, C. L., and Maury, O.: Influence of mesoscale eddies on biological production in the Mozambique Channel: Several contrasted examples from a coupled ocean-biogeochemistry model, Deep Sea Research Part II: Topical Studies in Oceanography, 100, 79-93, https://doi.org/10.1016/j.dsr2.2013.10.018, 2014.

José, Y. S., Dietze, H., and Oschlies, A.: Linking diverse nutrient patterns to different water masses within anticyclonic eddies in the upwelling system off Peru, Biogeosciences, 14(6), 1349-1364, https://doi.org/10.5194/bg-14-1349-2017, 2017.

Karstensen, J., B. Fiedler, F. Schütte, P. Brandt, A. Körtzinger, G. Fischer, R. Zantopp, J. Hahn, M. Visbeck, and D. Wallace.: Open Ocean Dead Zones in the Tropical North Atlantic Ocean, Biogeosciences 12 (8): 2597–2605, https://doi.org/10.5194/bg-12-2597-2015, 2015.

Karstensen, J., Schütte, F., Pietri, A., Krahmann, G., Fiedler, B., Grundle, D., ... and Visbeck, M.: Upwelling and isolation in oxygen-depleted anticyclonic modewater eddies and implications for nitrate cycling, Biogeosciences, 14(8), 2167-2181, https://doi.org/10.5194/bg-14-2167-2017, 2017.

Karstensen, J., Stramma, L., and Visbeck, M.: Oxygen minimum zones in the eastern tropical Atlantic and Pacific oceans, Progress in Oceanography, 77, 331–350, https://doi.org/10.1016/j.pocean.2007.05.009, 2008.

Keeling, R. F., Körtzinger, A., and Gruber, N.: Ocean deoxygenation in a warming world, Annual Review of Marine Science, 2(1), 199–229, https://doi.org/10.1146/annurev.marine.010908.163855, 2010.

Koné, N. V., Machu, E., Penven, P., Andersen, V., Garçon, V., Fréon, P., and Demarcq, H.: Modeling the primary and secondary productions of the southern Benguela upwelling system: A comparative study through two biogeochemical models, Global Biogeochemical Cycles, 19(4), https://doi.org/10.1029/2004GB002427, 2005.

Kostianoy, A. G., and I. M. Belkin.: A Survey of Observations on Intrathermocline Eddies in the World Ocean, Elsevier Oceanography Series 50 (C): 821–41, https://doi.org/10.1016/S0422-9894(08)70223-X, 1989.

Lam, Phyllis, Gaute Lavik, Marlene M. Jensen, Jack van de Vossenberg, Markus Schmid, Dagmar Woebken, Dimitri Gutiérrez, Rudolf Amann, Mike S. M. Jetten, and Marcel M. M. Kuypers.: Revising the Nitrogen Cycle in the Peruvian Oxygen Minimum Zone, Proceedings of the National Academy of Sciences 106 (12): 4752–57, https://doi.org/10.1073/PNAS.0812444106, 2009.

Llanillo, P. J., Pelegrí, J. L., Gasser, M., Emelianov, M., Gourrion, J., Rodríguez-Santana, A., and Duarte, C. M.: Meridional and zonal changes in water properties along the continental slope off central and northern Chile, Ciencias Marinas, 38(1B), 307-332, https://doi.org/10.7773/cm.v38i1B.1814, 2012.

Löscher, C. R., Fischer, M. A., Neulinger, S. C., Fiedler, B., Philippi, M., Schütte, F., ... and Schmitz, R. A.: Hidden biosphere in an oxygen-deficient Atlantic open-ocean eddy: future implications of ocean deoxygenation on primary production in the eastern tropical North Atlantic, Biogeosciences, 12(24), 7467-7482, doi:10.5194/bgd-12-14175-2015, 2015.

Lovecchio, E., Gruber, N., Münnich, M., and Frenger, I.: On the processes sustaining biological production in the offshore propagating eddies of the northern Canary Upwelling System, Journal of Geophysical Research: Oceans, 127(2), e2021JC017691, DOI:10.1029/2021jc017691, 2022.

Marshall, D. P., and Tansley, C. E.: An implicit formula for boundary current separation, Journal of physical oceanography, 31(6), 1633-1638, DOI:10.1175/1520-0485, 2001.

Matear, R. J., and Hirst, A. C.: Long-term changes in dissolved oxygen concentrations in the ocean caused by protracted global warming. Global Biogeochemical Cycles, 17(4), 1125, https://doi.org/10.1029/2002GB001997, 2003.

Mcwilliams, James C.: Submesoescale, coherent vortices in the ocean, Reviews of Geophysics 23(2): 165-182, https://doi.org/10.1029/RG023i002p00165, 1985.

Molemaker, M. Jeroen, James C. McWilliams, and William K. Dewar.: Submesoscale Instability and Generation of Mesoscale Anticyclones near a Separation of the California Undercurrent, Journal of Physical Oceanography 45 (3): 613–29, https://doi.org/10.1175/JPO-D-13-0225.1, 2015.

Montes, I., Dewitte, B., Gutknecht, E., Paulmier, A., Dadou, I., Oschlies, A., and Garçon, V.: High-resolution modeling of the Eastern Tropical Pacific oxygen minimum zone: Sensitivity to the tropical oceanic circulation, Journal of Geophysical Research: Oceans, 119(8), 5515-5532, DOI: 10.1002/2014JC009858, 2014.

Morales, C. E., Hormazabal, S., Correa-Ramirez, M., Pizarro, O., Silva, N., Fernandez, C., ... and Torreblanca, M. L.: Mesoscale variability and nutrient–phytoplankton distributions off central-southern Chile during the upwelling season: The influence of mesoscale eddies, Progress in Oceanography, 104, 17-29, https://doi.org/10.1016/j.pocean.2012.04.015, 2012.

Morel, A., and Berthon, J. F.: Surface pigments, algal biomass profiles, and potential production of the euphotic layer: Relationships reinvestigated in view of remote-sensing applications, Limnology and oceanography, 34(8), 1545-1562, https://doi.org/10.4319/lo.1989.34.8.1545, 1989.

Naqvi, S. W. A., Bange, H. W., Farías, L., Monteiro, P. M. S., Scranton, M. I., and Zhang, J.: Marine hypoxia/anoxia as a source of CH_4 and N_2O, Biogeosciences, 7(7), 2159-2190, https://doi.org/10.5194/bg-7-2159-2010, 2010.

Oschlies, A., Brandt, P., Stramma, L., and Schmidtko, S.: Drivers and mechanisms of ocean deoxygenation, Nature Geoscience, 11(7), 467–473, https://doi.org/10.1038/s41561-018-0152-2, 2018.

Paulmier, A., Ruiz-Pino, D., Garçon, V., and Farias, L.: Maintaining of the East South Pacific Oxygen Minimum Zone (OMZ) off Chile, Geophysical Research Letters, 33, L20601, https://doi.org/10.1029/2006GL026801, 2006.

Pegliasco, Cori, Alexis Chaigneau, and Rosemary Morrow.: Main Eddy Vertical Structures Observed in the Four Major Eastern Boundary Upwelling Systems, Journal of Geophysical Research: Oceans 120 (9): 6008–33, https://doi.org/10.1002/2015JC010950, 2015.

Pena, M. A., Katsev, S., Oguz, T., and Gilbert, D.: Modeling dissolved oxygen dynamics and hypoxia, Biogeosciences, 7(3), 933-957, https://doi.org/10.5194/bg-7-933-2010, 2010.

Pitcher, G. C., Aguirre-Velarde, A., Breitburg, D.,... and Zhu, ZY.: System controls of coastal and open ocean oxygen depletion, Progress in Oceanography, Volume 197, https://doi.org/10.1016/j.pocean.2021.102613, 2021.

Pizarro-Koch, M., Pizarro, O., Dewitte, B., Montes, I., Ramos, M., Paulmier, A., and Garçon, V.: Seasonal variability of the southern tip of the Oxygen Minimum Zone in the eastern South Pacific (30-38 S): A modeling study, Journal of Geophysical Research: Oceans, 124(12), 8574-8604, https://doi.org/10.1029/2019JC015201, 2019.

Sarmiento, J. L., and Gruber, N.: Sinks for anthropogenic carbon, Physics today, 55(8), 30-36, DOI:10.1063/1.1510279, 2002.

Sarmiento, J. L., and Gruber, N.: Ocean biogeochemical dynamics, Princeton university press, 528 pp., ISBN 9780691017075, 2006.

Schütte, F., Brandt, P., and Karstensen, J.: Occurrence and characteristics of mesoscale eddies in the tropical northeastern Atlantic Ocean, Ocean Science, 12(3), 663-685, https://doi.org/10.5194/os-12-663-2016, 2016.

Shchepetkin, A. F., and McWilliams, J. C.: The regional oceanic modeling system (ROMS): a split-explicit, free-surface, topography-following-coordinate oceanic model, Ocean modelling, 9(4), 347-404, https://doi.org/10.1016/j.ocemod.2004.08.002, 2005.

Schmidtko, S., Stramma, L. and Visbeck, M.: Decline in global oceanic oxygen content during the past five decades, Nature 542, 335–339, https://doi.org/10.1038/nature21399, 2017.

Smith, R. D., Dukowicz, J. K., and Malone, R. C.: Parallel ocean general circulation modeling, Physica D: Nonlinear Phenomena, 60(1-4), 38-61, https://doi.org/10.1016/0167-2789(92)90225-C, 1992.

Stramma, L., H. W. Bange, R. Czeschel, A. Lorenzo, and M. Frank.: On the Role of Mesoscale Eddies for the Biological Productivity and Biogeochemistry in the Eastern Tropical Pacific Ocean off Peru, Biogeosciences 10 (11): 7293–7306, https://doi.org/10.5194/bg-10-7293-2013, 2013.

1185 Stramma, Lothar, Robert Weller, Rena Czeschel, and Sebastien Bigorre.: Eddies and an Extreme Water mass
1186 Anomaly Observed in the Eastern South Pacific at the Stratus mooring, Journal of Geophysical Research:
1187 Oceans 118: 3114–27, https://doi.org/10.1002/jgrc.20224, 2014.

1188 Stramma, L., Schmidtko, S., Levin, L. A., and Johnson, G. C.: Ocean oxygen minima expansions and their
1189 biological impacts, Deep Sea Research Part I: Oceanographic Research Papers, 57, 587–595,
1190 https://doi.org/10.1016/j.dsr.2010.01.005, 2010.

1191 Suntharalingam, P., Sarmiento, J. L., and Toggweiler, J. R.: Global significance of nitrous-oxide production
1192 and transport from oceanic low-oxygen zones: A modeling study, Global Biogeochemical Cycles, 14(4),
1193 1353-1370, https://doi.org/10.1029/1999GB900100, 2000.
1194
1195 Suntharalingam, P., Buitenhuis, E., Le Quéré, C., Dentener, F., Nevison, C., Butler, J. H., ... and Forster, G.:
1196 Quantifying the impact of anthropogenic nitrogen deposition on oceanic nitrous oxide, Geophysical Research
1197 Letters, 39(7), https://doi.org/10.1029/2011GL050778, 2012.

1198 Thomsen, S., Kanzow, T., Krahmann, G., Greatbatch, R. J., Dengler, M., and Lavik, G.: The formation of a
1199 subsurface anticyclonic eddy in the Peru-Chile Undercurrent and its impact on the near-coastal salinity,
1200 oxygen, and nutrient distributions, Journal of Geophysical Research: Oceans, 121(1), 476-501, doi:10.1002/
1201 2015JC010878, 2016.

1202 Ulloa, O., Canfield, D. E., DeLong, E. F., Letelier, R. M., and Stewart, F. J.: Microbial oceanography of
1203 anoxic oxygen minimum zones, Proceedings of the National Academy of Sciences, 109(40), 15996–16003,
1204 https://doi.org/10.1073/pnas.1205009109, 2012.

1205 Vergara, O., Dewitte, B., Montes, I., Garçon, V., Ramos, M., Paulmier, A., and Pizarro, O.: Seasonal
1206 variability of the oxygen minimum zone off Peru in a high-resolution regional coupled model,
1207 Biogeosciences, 13(15), 4389-4410, https://doi.org/10.5194/bg-13-4389-2016, 2016.

1208 Wright, Jody J., Kishori M. Konwar, and Steven J. Hallam.: Microbial Ecology of Expanding Oxygen
1209 Minimum Zones, Nature Reviews Microbiology 10 (6): 381–94, https://doi.org/10.1038/nrmicro2778, 2012.

1210 Wyrtki, K.: The oxygen minima in relation to ocean circulation, Deep Sea Res, Oceanogr. Abstr., 9, 11–23,
1211 https://doi.org/10.1016/0011-7471(62)90243-7, 1962.

1212 Yakushev, E. V., Pollehne, F., Jost, G., Kuznetsov, I., Schneider, B., and Umlauf, L.: Analysis of the water
1213 column oxic/anoxic interface in the Black and Baltic seas with a numerical model, Marine Chemistry,
1214 107(3), 388-410, https://doi.org/10.1016/j.marchem.2007.06.003, 2007.

1215

1216